AD-A216 549

REPORT DOCUMENTATION PAGE

Form Approved
OMB No. 0704-0188

1. AGENCY USE ONLY (Leave blank)	2. REPORT DATE	3. REPORT TYPE AND DATES COVERED
	Nov 30, 1983	Final (Oct 1, 1982-Sept 30, 1983

4. TITLE AND SUBTITLE
METALLIC GLASSES: INVESTIGATION OF THE ELECTRONIC STRUCTURE AND ITS RELATIONSHIP TO PHYSICAL PROPERTIES

5. FUNDING NUMBERS
61102F
2306/C3

6. AUTHOR(S)
William A. Hines

7. PERFORMING ORGANIZATION NAME(S) AND ADDRESS(ES)
Department of Physics and Institute of Materials Science, University of Connecticut
Storrs, Connecticut 06268

8. PERFORMING ORGANIZATION REPORT NUMBER
AFOSR-TR- 89-1772

9. SPONSORING/MONITORING AGENCY NAME(S) AND ADDRESS(ES)
AFOSR
BLDG 410
BAFB DC 20332-6448

10. SPONSORING/MONITORING AGENCY REPORT NUMBER
AFOSR-80-0030

11. SUPPLEMENTARY NOTES

12a. DISTRIBUTION/AVAILABILITY STATEMENT
Approved for public release;
distribution unlimited.

12b. DISTRIBUTION CODE

13. ABSTRACT (Maximum 200 words)

20. ABSTRACT (Continue on reverse side if necessary and identify by block number)

This report summarizes the work which was completed during the first three years of the research program (October 1, 1979 to September 30, 1981). Included are: (1) a NMR and magnetic susceptibility study of several rapidly quenched Ni-Pd-P, Ni-Pt-P and Ni-P metallic glasses, (2) a magnetization study of the $RE_{100-x}Al_x$ amorphous alloys (where RE is a rare earth element), (3) a NMR, magnetization and x-ray diffraction study of crystalline $Fe_{3-x}Ni_xSi$ and Metglas 2605 CO ($Fe_{67}Co_{18}B_{14}Si_1$), (4) a NMR and magnetic susceptibility study o

14. SUBJECT TERMS

15. NUMBER OF PAGES
58

16. PRICE CODE

17. SECURITY CLASSIFICATION OF REPORT	18. SECURITY CLASSIFICATION OF THIS PAGE	19. SECURITY CLASSIFICATION OF ABSTRACT	20. LIMITATION OF ABSTRACT
unclassified	unclassified		

the $Ca_{100-x}Al_x$ metallic glass system and (5) a magnetization study of some)Nb-B and Fe-Nb-B metallic glasses. In addition, this report describes in complete detail the progress during the past year (October 1, 1982 to September 30, 1983) which includes: (1) a pulse NMR study of the atomic and electronic structures of the Ca-Al metallic glass system, (2) a study of the density of unoccupied d states in transition metal + metalloid metallic glasses and (3) an EXAFS study of Metglas 2605 CO. Abstracts from this work follow.

In order to investigate the atomic and electronic structures, pulse NMR experiments were carried out on ^{27}Al in the melt spun $Ca_{100-x}Al_x$ metallic glass system and the related crystalline compounds. The spin-echo quadrupole spectra indicate considerable distribution in the electric field gradient and non-uniaxial local symmetry for the Al atoms. Measurements of the spin-lattice relaxation time are consistent with a small density of s-electron states at the Al sites as predicted by recent band structure calculations.

New data on the x-ray absorption edge near-in structure of the $(Ni_{0.50}Pt_{0.50})_{75}P_{25}$ system is compared with previous results on random solid solution alloys and other TM + G metallic glasses. Whereas experimental probes of the density of d states at the Fermi energy, $\rho_d(E_f)$, often indicate a sharp reduction in $\rho_d(E_f)$ due to the presence of metalloids or non-transition metals, absorption edge results usually indicate a negligible decrease in the total number of d holes per transition metal atom. In the $(Ni_{0.50}Pt_{0.50})_{75}P_{25}$ system the number of 5d holes per Pt site is actually found to be greater than for the case of pure Pt. A model is proposed which may reconcile the results of absorption edge measurements and $\rho_d(E_f)$ determinations.

The environment of the Fe and Co sites in Metglas 2605 CO ($Fe_{67}Co_{18}B_{14}Si_1$) has been investigated by the EXAFS technique. Studies were conducted on alloys subjected to a magnetic anneal, as well as alloys in the as fabricated condition. The EXAFS measurements were carried out with x-ray polarization directions parallel and perpendicular to the ribbon direction. It is found that the average distance from a Co site to the first transition metal coordination shell is always less than the corresponding distance for an Fe site. In addition, upon comparing data taken at room temperature with that collected at nitrogen temperature, an anisotropic behavior is detected in the fractional change in disorder.

Finally, this report describes the status of experiments currently in progress which includes: (1) optical properties of Ni-P metallic glasses and (2) a spin-echo NMR study of atomic environment in the $Fe_{100-x}B_x$ metallic glass system. The course of future work is also discussed.

Grant Number: AFOSR 80-0030

William A. Hines
Department of Physics and Institute of Materials Science
University of Connecticut
Storrs, Connecticut 06268

November 30, 1983

Interim Scientific Report: October 1, 1982 to September 30, 1983

METALLIC GLASSES: INVESTIGATION OF THE ELECTRONIC STRUCTURE AND ITS RELATIONSHIP TO PHYSICAL PROPERTIES

Prepared for the United States Air Force, Air Force Office of Scientific Research, Bolling Air Force Base, Building 410, Washington, DC 20332

AFOSR-TR- 89-1772

I. INTRODUCTION

During the past decade, materials scientists and solid state physicists have devoted considerable research activity to amorphous materials such as magnetic glasses, amorphous semiconductors and amorphous metallic alloys[1-3]. This is due to a combination of a desire for a re-examination of some fundamental concepts of solids as well as the possibility for a variety of technological applications[4]. Our research effort has focused principally on the class of amorphous materials known as "amorphous metallic alloys" or "metallic glasses"; materials which possess all the properties normally associated with metals but are not spatially periodic. For the most part, we have studied metallic glass systems with the general form $TM_{100-x}G_x$, where TM is a transition metal (or combination of transition metals) such as Ni, Pd, Pt, Fe or Co; and G is a high valence metalloid (or combination of metalloids) such as B, Nb, Si or P. Although there are several methods of preparation, these amorphous alloys are typically prepared by rapid quenching ($\sim 10^5$ to 10^7 °C/sec) from the liquid state and possess metalloid compositions ranging from x = 15 to 30 at. %. Recently, because of their special significance, we have included systems of the form $RE_{100-x}M_x$ and $M^1_{100-x}M^2_x$, where RE is a 4f rare earth element such as Ce, Pr or Dy; and M is a simple metal such as Ca or Al. Our research program utilizes the techniques of nuclear magnetic resonance (pulse and steady state), magnetization, specific heat, optical spectroscopy, x-ray diffraction and x-ray absorption (near-in and EXAFS), in the study of: (1) the electronic structure, (2) the amorphous (glassy) structure, (3) the crystallization and (4) the bonding, glass forming tendency and structural stability of metallic glasses. This in turn leads to a better understanding of the electronic, magnetic and mechanical properties for these materials. In particular, our primary concern is a determination of the electronic structure (e.g., den-

sity of states) and its relationship to the technically useful physical properties. Finally, nuclear magnetic resonance and magnetization experiments are being used to investigate (5) the occurrence and size of localized moments, the degree of spin polarization, the magnetic moment interactions (applied field, exchange and anisotropy), and the nature of any magnetic ordering. The results are being compared with existing theories of magnetism in amorphous materials.

The Air Force Office of Scientific Research (AFOSR) commenced sponsorship of this program on October 1, 1979. This Interim Scientific Report describes generally the progress which has been made during the four years of the supported program with specific emphasis on this past year (October 1, 1982 to September 30, 1983). The progress is discussed in the context of our proposed objectives. To date, eleven journal articles, seven abstracts and eighteen oral presentations can be credited to the AFOSR support of this program.

Sections IIA, IIB and IIC consist of concise one page statements which describe the "Objectives of Program", "Methods of Approach" and "Statement of Work", respectively. Such summary statements were contained in the previous proposal. Section III summarizes the scientific progress achieved during the first three years of the research program. Section IV ("Atomic and Electronic Structures of the Ca-Al Metallic Glass System: A Pulse NMR Study"), Section V ("On the Density of Unoccupied d States in Transition Metal + Metalloid Metallic Glasses"), Section VI ("EXAFS Study of Metglas 2605 CO") and Section VII ("Other Work") describe in detail the progress achieved during the past year. Section VIII lists all of the journal articles, abstracts and oral presentations which can be credited to AFOSR support while Section IX briefly describes the course of future work.

II. SUMMARY STATEMENTS

A. Objectives of Program

The goals of the proposed work are to determine the electronic structure of metallic glasses and to investigate its relationship to the physical properties. In particular, the first objective is to quantitatively investigate the nature of the electronic density of states for metallic systems which have no long range crystallographic order. The experiments will distinguish between various approaches, ranging from liquid metal theories (which involve the nearly free electron approximation and pseudopotential techniques) to near neighbor environment models, as well as determine the applicability of rigid band ideas. Secondly, it is proposed to test certain features of the dense random packing model or, perhaps, support an alternative model (e.g., the random packing of microcrystalline units) for the atomic structure of metallic glasses. The experiments will determine the role of atomic size and electronegativity in such a structure. Thirdly, it is the objective of the proposed work to investigate the process of crystallization. In addition to identifying the resulting phases, the experiments will determine how near neighbor environments are affected by the thermal, magnetic and mechanical history. Fourthly, it is proposed to investigate the nature of bonding, structural stability and glass forming tendency for metallic glasses in the light of current theoretical descriptions. Such descriptions include an ionic-like charge transfer, directional covalent bonding and a lowering of the density of states. Finally, it is proposed to examine existing theories of magnetism in amorphous materials concerning the occurrence and size of localized moments, spin polarization, magnetic interactions (applied field, exchange and anisotropy), and magnetic ordering. All of this will lead to a better understanding of the electronic, magnetic and mechanical properties for metallic glasses.

B. Approaches and Techniques

During the course of the research program, the experimental approach will utilize the tools of nuclear magnetic resonance (pulse and steady state), magnetization, specific heat, optical spectroscopy, x-ray diffraction and x-ray absorption (near-in and EXAFS) in the study of metallic glasses having the general forms $TM_{100-x}G_x$ and $M^1_{100-x}M^2_x$. Above, TM represents a transition metal (or combination) such as Ni, Pd, Pt, Fe or Co; G represents a high valence metalloid glass former (or combination) such as B, Nb, Si or P; and M represents a simple metal such as Ca or Al. These alloys possess favorable NMR species and are readily available in the amorphous state with compositions which can be systematically varied. Also, the magnetic properties of an additional system of the form $RE_{100-x}Al_x$, where RE represents a 4f rare earth element, will be included.

Initially, the NMR Knight shift, NMR spin-lattice relaxation rate and magnetic susceptibility were heavily exploited since they provide a direct picture of the electronic structure. Now, the research program has been expanded to include specific heat, specular reflectivity and near-in x-ray absorption experiments which not only support the NMR results, but also provide a quantitative calculation for the s- and d-band densities of states. The description of the electronic structure which is being obtained will enable an understanding of several physical properties (e.g., structural stability). Furthermore, NMR linewidth, EXAFS and x-ray diffraction measurements are providing information concerning the near neighbor environment and, hence, can be utilized to probe the atomic structure and how it is affected by thermal, magnetic and mechanical processes. Using systematic variations in composition, the role of atomic size and electronegativity are being determined. Finally, magnetization measurements are providing information concerning the size and occurrence of localized moments, degree of spin polarization, magnetic interactions, and nature of magnetic ordering; all of which can be compared with existing theories of magnetism in amorphous materials.

C. Statement of Work

This program represents a systematic and detailed investigation of the electronic structure of metallic glasses and its relationship to the physical properties. The techniques being utilized include nuclear magnetic resonance, magnetization, specific heat, optical spectroscopy, x-ray diffraction and x-ray absorption. This section constitutes a statement of specific research work to be carried out by the Principal Investigator during the course of the supported program. Using the tools outlined above, the Principal Investigator will:

(1) determine the nature of the electronic structure for metallic glasses, including a quantitative evaluation for the s- and d-band densities of states and hyperfine coupling constants,

(2) investigate the applicability of such approaches as the nearly free electron models, liquid metal theories, near neighbor models and rigid band ideas to the electronic structure for metallic glasses,

(3) determine the relationship between the electronic structure for metallic glasses and such physical properties as bonding, structural stability and glass forming tendency,

(4) investigate the nature of the atomic structure for metallic glasses (in the light of dense random packing and microcluster models) and determine the role played by such parameters as atomic size and electronegativity,

(5) determine how near neighbor atomic environments are affected by the thermal, magnetic and mechanical history, and investigate the phases resulting from crystallization,

(6) investigate the occurrence and size of localized moments, degree of spin polarization, magnetic interactions (applied field, exchange, anisotropy), and nature of magnetic ordering; compare the results with existing theories of magnetism in amorphous materials.

This proposed work will lead to a better understanding of the electronic, magnetic and mechanical properties for metallic glasses.

III. PROGRESS AND ACHIEVEMENTS (First Three Years of Research Program)

This section summarizes the general progress achieved during the first three years of the research program (October 1, 1979 to September 29, 1982). A list of publications resulting from the program is provided in Section VIII. Preprints and reprints of the publications have been submitted to the AFOSR under separate cover.

A. NMR and Magnetic Susceptibility Study of the Ni-Pd-P, Ni-Pt-P and Ni-P Metallic Glass Systems

During the first three years of the research program, extensive NMR and magnetic susceptibility experiments were carried out on several rapidly quenched metallic glasses from the transition metal + metalloid family. By systematically varying the composition in the Ni-Pd-P, Ni-Pt-P and Ni-P metallic glasses, a preliminary qualitative description of the electronic structure was obtained. Publications A1, A3, A4 and B1 (see Section VIII) describe in detail the NMR and magnetic susceptibility work which was carried out on the systems above. Here, we will summarize the important scientific conclusions from the work on these systems which have implications for the $TM_{100-x}G_x$ metallic glass systems in general. The metalloid (^{31}P) Knight shift and spin-lattice relaxation rate for all of these systems depend only on the P concentration, x, and not the relative transition metal composition (i.e., what fraction of Ni atoms are replaced by Pd or Pt). The ^{31}P Knight shift and spin-lattice relaxation rate are attributed solely to the direct contact hyperfine interaction. On the other hand, the transition metal (^{195}Pt) Knight shift has contributions arising from both the direct contact hyperfine and core polarization interactions, and depends on both the metalloid concentration and relative transition metal composition. The results are discussed in terms of a rigid two-band picture with estimates being made for the s- and d-band densities of states and hyperfine coupling

constants. Relative to the Fermi energy, the d-states associated with Ni are higher in energy (and, therefore, the number of d-holes is greater), than those for Pd and Pt. Consistent with the DRP model, there is evidence of a transfer of charge from the P metalloid atoms to the transition metal d-states in these systems. For the $(Ni_{0.50}Pd_{0.50})_{100-x}P_x$ system, these states become full for $x \tilde{\sim} 20$. Since the rigid band model predicts that if all of the P electrons go into the d-states, the filling would be complete for $x \tilde{\sim} 11$, we conclude that slightly more than half of the P electrons go into the conduction band. There is no evidence of any minimum in the density of states as predicted by Nagel and Tauc[5]. Finally, we note that the various ^{31}P Knight shift and relaxation rate values satisfy Korringa relationships, with the value of the experimental Korringa constant decreasing as the P concentration increases. The values range from two to three times the free-electron value.

B. Magnetization Study of the $RE_{65}Al_{35}$ Metallic Glass Systems

Because of the existence of highly localized magnetic moments, the magnetic properties of rare earth + simple metal metallic glasses are of particular interest. Measurements of the bulk magnetization have been made as a function of temperature and magnetic field for three amorphous alloys from the $RE_{100-x}Al_x$ series: $Ce_{65}Al_{35}$, $Pr_{65}Al_{35}$ and $Dy_{65}Al_{35}$. Publication A6 describes this work in detail with the following scientific conclusions. $Dy_{65}Al_{35}$ and $Pr_{65}Al_{35}$ demonstrate a behavior which is characteristic of ferromagnetic ordering, without the implication of a strictly parallel alignment of moments. The onset of hysteresis and relaxation effects below the ordering temperature, as well as the lack of saturation, provides evidence of strong local anisotropy. Such behavior has been described by Ferrer and Zuchermann[6] using a random magnetic anisotropy model. Evidence for a RKKY interaction comes from the negative Curie-Weiss value for

$Ce_{65}Al_{35}$. This result appears to contradict the work of Buschow[7] on amorphous Gd alloys in which it was concluded that the RKKY interaction was of minor importance.

C. NMR, Magnetization and X-Ray Diffraction Study of the $Fe_{3-x}Ni_xSi$ Crystalline and $Fe_{67}Co_{18}B_{14}Si_1$ Metallic Glass Systems

Spin-echo NMR, magnetization and x-ray diffraction studies on the crystalline $Fe_{3-x}Ni_xSi$ system have enabled us to correlate magnetic moment formation and hyperfine field interactions with local (short range) environment configurations. Such studies on crystalline binary and ternary systems based on Fe_3Si are relevant to $TM_{100-x}G_x$ metallic glasses due to similarities in the atomic and electronic structures. The NMR results demonstrated that Ni selectively replaces the Fe in one of the two Fe-sites inherent in the Fe_3Si structure and, consequently, a local environment model relating the hyperfine fields with the magnetic moments previously developed for such systems can be applied[8]. When one uses this model, a subdivision of the observed internal fields into contributions arising from the 4s spin polarization transferred from neighboring moments and the polarization resulting from the on-site moments is obtained. This work is described in detail in publication A2.

Similar experiments were carried out on the $Fe_{67}Co_{18}B_{14}Si_1$ (Metglas 2605 CO) metallic glass which yielded information concerning the near neighbor atomic environment and how it is affected by magnetic annealing. Spin-echo NMR spectra obtained from both metalloid (^{11}B) and transition metal (^{59}Co) nuclei detected no significant difference between an as-fabricated sample and a sample which has undergone the appropriate magnetic annealing for yielding the extremely high magnetomechanical coupling constants found in these systems[9]. Hence, it was concluded that any anisotropic atomic rearrangement which occurs during such magnetic annealing processes must

involve a relatively small number of atoms, or be so subtle, that no significant change occurs in the broad NMR spectra obtained from amorphous materials. This is consistent with the prediction of Graham and Egami[10]. We note, however, that very recent and preliminary EXAFS experiments on the same samples do indicate an atomic rearrangement (see publication B7 and Section VI in this report). Careful x-ray diffraction studies indicate that a thin crystalline surface layer, which extends into the ribbon $\lesssim$ 3 μm, occurs on only the substrate wheel side of the as-fabricated ribbon. Most of the crystallites consist of an α-Fe phase and are preferentially oriented in a fiber texture configuration; the fiber axis being a mixture of the [100] and [110] directions, and normal to the ribbon surface. The crystalline surface layer does not appear to influence the high value of the magnetomechanical coupling factor obtained through magnetic annealing. This work is described in detail in publications A5, A9 and B6. A very recent reprint (publication A9) concerning the surface crystallinity is included at the end of this section.

D. NMR and Magnetic Susceptibility Study of the $Ca_{100-x}Al_x$ Metallic Glass System

Steady state NMR and magnetic susceptibility experiments have been carried out on a new metallic glass system consisting of "simple" metals only. A reprint (publication A8) describing these initial results is included at the end of this section. Due to the existence of a nuclear quadrupole moment and differences in valence, $Ca_{100-x}Al_x$ ($15 \leq x \leq 45$ at. %) is ideal for studies of both the atomic and electronic structures. ^{27}Al NMR spectra were observed at room temperature as a function of resonance frequency for the various compositions. A consideration of the intensity, shape and frequency dependence indicates that the line is due to the central component only, or +1/2 $\longleftrightarrow$ -1/2 transition, with the other transi-

tions being far removed from the line due to the first order quadrupole interaction (see Fig. 1 in the reprint). Furthermore, both the ^{27}Al Knight shift and linewidth remain unchanged as the composition is varied throughout the entire glassy regime (see Figs. 2 and 3, respectively, in the reprint). Since both the average electronic concentration and average atomic volume change appreciably, these results provide evidence that certain features of the nearest neighbor atomic environment and electronic structure remain fixed as the composition is varied (i.e., some form of short range order). We note that for the transition metal + metalloid systems studied (see Section IIIA), the (^{31}P) metalloid Knight shift decreases dramatically as the electronic concentration is increased. Also, for the same $TM_{100-x}G_x$ systems, the linewidth is very sensitive to composition. Finally, an analysis of the composition dependence for the room temperature magnetic susceptibility (see Fig. 4 in the reprint) indicates that estimates based on the free electron model are inadequate.

E. Magnetization Study of the Co-Nb-B and Fe-Nb-B Metallic Glass Systems

Measurements of the saturation magnetization (and hence, Co or Fe magnetic moment) as well as the Curie temperature have been carried out on several new amorphous metallic alloys based on Co or Fe and stabilized with up to 10 at. % B and 14 at. % Nb. These new systems show attractive soft ferromagnetic properties, similar to those of the familiar transition metal + metalloid systems, while offering improved thermal stability despite the reduced metalloid content. This work is described in detail in publications A7, B2 and B3. A recent reprint (publication A7) is included at the end of this section.

Study of the crystalline surface of Metglas 2605 CO [a)]

M. Choi,[b)] D. M. Pease, W. A. Hines, J. I. Budnick, and G. H. Hayes
Institute of Materials Science, University of Connecticut, Storrs, Connecticut 06268

L. T. Kabacoff
Naval Surface Weapons Center, White Oak, Silver Spring, Maryland 20910

(Received 3 February 1983; accepted for publication 6 April 1983)

X-ray studies using a diffractometer and Read camera are reported for Metglas 2605 CO. A crystalline surface layer, which extends into the sample $\lesssim 3\,\mu$m occurs on only the substrate wheel side of the as-quenched ribbon. Most of the crystallites consist of an α-iron phase and are preferentially oriented in a fiber texture configuration; the fiber axis being a mixture of the [100] and [110] directions, and normal to the ribbon surface. A small amount of non α-iron crystallinity is also present. The crystalline surface layer does not appear to influence the high value of the magnetomechanical coupling factor obtained through magnetic annealing.

PACS numbers: 61.10.Fr, 61.55.Hg, 75.50.Kj, 75.80. + q

Recently, there has been considerable research interest concerning metallic glasses with enhanced magnetomechanical coupling factors k_{33}, a factor which is a measure of the efficiency of conversion of magnetic energy into elastic energy. In particular Metglas 2605 CO ($Fe_{67}Co_{18}B_{14}Si_1$) and Metglas 2605 SC ($Fe_{81}B_{13.5}Si_{13.5}C_2$) exhibit very high coupling factors (0.71 and $\gtrsim 0.9$, respectively) after undergoing specific magnetic annealing treatments.[1] During the course of a recent spin-echo nuclear magnetic resonance study of Metglas 2605 CO, it was discovered that a thin layer (< 5 μm) of surface crystallinity existed on the side of the as-quenched ribbon which was closest to the substrate wheel during the fabrication process.[2] In order to ascertain the relationship between near neighbor atomic environment and useful magnetoelastic properties for this material, it seemed that a necessary prerequisite would be to investigate the nature of the surface crystallinity, and how this crystallinity is effected by annealing treatments.

There are several studies showing differences in crystallization behavior upon annealing for the wheel versus nonwheel sides of several metallic glasses.[3–6] However, as of this writing, the only study of surface crystallinity in a metallic glass resulting directly from the fabrication process is the report by Davis *et al.*[7] concerning the wheel side surface crystallinity in Metglas 2605 S ($Fe_{82}B_{12}Si_6$). They attribute the crystallinity to the oxidation of boron by air trapped in the "valley" regions of the irregular wheel side surface, so that a depletion of boron from the top 1 000 Å of these regions removes the local composition from the glass forming regime. Davis *et al.*[7] indicate that the resulting crystallinity is probably limited to the valley regions of the sample. Subsequent to the discovery of the surface crystallinity, Metglas 2605 S was modified to include carbon. The resulting modification is the well-known composition 2605 SO, and Davis *et al.*[7] suggest the added carbon may play some role in protecting the boron from oxidation and inhibiting the crystallization. In the present work, we report surface crystallinity on the wheel (or "dull") side of Metglas 2605 CO. Furthermore, we demonstrate, for the first time, the existence of a "fiber texture" type of preferred orientation in the surface crystallites of an as-quenched metallic glass.

Ribbons, 1.3 cm wide and 40 μm thick, of Metglas 2605 CO prepared by the "planar flow casting" process are commercially available from the Allied Corporation.[8] The three types of sample ribbon used in this study were the same as those used in the earlier spin-echo NMR work[2] and have undergone the following annealing treatments: (1) no annealing treatment after the initial fabrication; (2) annealing at 369 °C in a magnetic field of 6.1 kOe which lies in the plane of the ribbon and transverse to its length; (3) annealing at 427 °C in a magnetic field of 6.1 kOe which lies in the plane of the ribbon and transverse to its length. The sample prepared from the original material [(1) above] is designated as quenched. The sample prepared by process (2) is designated annealed, and yields a value of k_{33} near the maximum attainable for Metglas 2605 CO. The sample represented by (3) is designated crystalline and has a drastically reduced value of k_{33}.

X-ray diffraction studies were carried out using a diffractometer and a Read camera. The diffractometer was outfitted with a monochromator and used in conjunction with a copper target x-ray tube. The copper K_α emission line exceeds in energy the iron and cobalt K edges and is highly absorbed in 2605 CO Metglas; thus, the diffractometer scans were sensitive to the top few microns only. The diffractometer results were complimented by glancing angle x-ray diffraction studies using a Read camera. In these experiments, a ten degree glancing angle and a 0.25-mm beam collimator were used. Filtered radiation from a cobalt target x-ray tube was used in the glancing angle studies.

Diffractometer scans were carried out on samples which were progressively thinned, using a metallography polishing wheel and various Al_2O_3 slurries, in order to ascertain variations in structural characteristics with depth. Read camera exposures were carried out using different orientations (0°, 37°, 90°, and 180°) of the ribbon about an axis normal to its surface in order to test whether or not the crystal-

[a)] Work at the University of Connecticut supported by the AFOSR (80-0030) and at the Naval Surface Weapons Center by NAVAIR (WF 615420).

[b)] Contributions of M. Choi are from thesis material submitted in partial fulfillment of the requirements of the Ph.D. degree at the University of Connecticut.

 0021-8979/83/074193-04$02.40

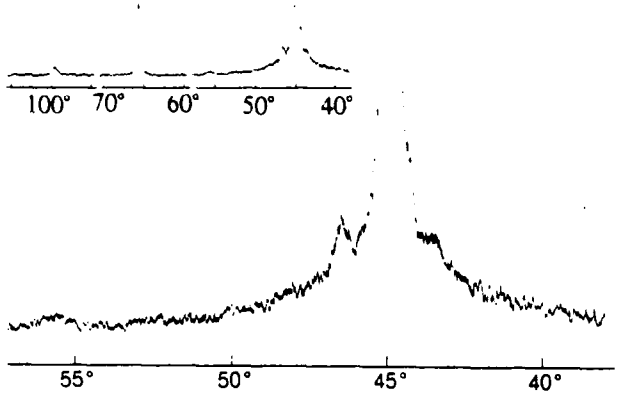

FIG. 1. X-ray diffractometer scan for the substrate wheel side of "as quenched" Metglas 2605 CO showing three bcc α-Fe peaks [$2\theta = 45.0°$, 65.5°, 99.7°, or (110), (200), (220), respectively] and four "boride phase" peaks [$2\theta = 43.5°$, 44.3°, 46.5°, 55.8°].

line fiber axis was perpendicular to the ribbon surface. In addition to the x-ray diffraction studies, the as-quenched ribbon was characterized using a scanning electron microprobe which was capable of detecting the boron K_α emission line, as well as the cobalt and iron K_α lines emitted by the sample elements. Finally, profilometer measurements were made on the as-quenched ribbon.

Figure 1 shows an x-ray diffractometer scan which was taken from the wheel side of the as-quenched ribbon. Three crystalline peaks are clearly visible. These peaks correspond to the (110), (200), and (220) peaks of an α-iron phase; however, the (211) and (310) peaks are missing. The diffractometer is capable of detecting reflections from only those planes parallel to the ribbon surface, and will not detect the presence of sets of planes which are excluded from being parallel to the surface because of preferred orientation. Table I lists the results from all the x-ray diffractometer scans which were taken from both the wheel (or dull) and opposite-the-wheel (or shiny) sides of all three sample ribbons. We note that the shiny side of the as-quenched ribbon demonstrated a diffraction pattern characteristic of a completely amorphous material while the shiny side of the annealed ribbon possessed traces of crystallinity.

A Read camera photograph was taken from the dull side of the as-quenched ribbon. Unlike the diffractometer scan described above, five diffraction rings corresponding to the α-iron phase appeared; i.e., there were no missing reflections. More significantly, intense pairs of arcs were observed on the (110) ring which indicate a fiber texture orientation of the crystallites (see Fig. 2). By measuring the coordinates of the intense arcs and solving the geometry corresponding to the Read camera reflection conditions, one can determine the angles between the normal to the sample surface and the (110) plane which reflects x-rays into a point on the arc.[9] The angles corresponding to the two intense arcs are 45° and 60°. These angles are the values expected if planes of the {100} and {110} form are parallel to the surface. By measuring the fiber texture arcs for 180° rotations of the sample, it was demonstrated that the mixed [110] and [100] fiber axes were normal to the ribbon surface. It is to be noted that a mixed [110] and [100] fiber texture is consistent with the diffractometer results.

In addition to the intense peaks corresponding to an α-iron phase, the diffractometer scan of the dull side of the as-quenched sample shows four small additional peaks. One peak matches closely the (321) reflection of body-centered-tetragonal (bct) Fe_3B studied by Walter, Bartram, and Russell,[10] and the other three peaks match approximately other strong peaks observed by those authors. However, our results show no evidence of the strong (411) reflection of bct Fe_3B. A comparison between the reflections observed in the

TABLE I. X-ray diffraction data for crystalline phases in Metglas 2605 CO (d spacings in Å).

As-quenched dull side	As-quenched shiny side	Annealed dull side	Annealed shiny side	Crystalline dull side	Crystalline shiny side	Best fit[a]
2.083	...	2.085	...	2.083	...	2.088 Fe_3B (321)
2.047	...	2.047	...	2.042	...	2.028 Fe_3B (330) and (112)
2.017	...	2.017	2.023	2.021	2.021	2.027 α-Fe (110)
1.953	...	1.953	...	1.961	...	1.930 Fe_3B (420) and (202)
1.647	...	1.650	...	1.653	...	1.690 Fe_3B (510) and (312)
1.425	...	1.425	1.429	1.430	1.431	1.433 α-Fe (200)
Missing	...	1.169	1.169	1.169	1.169	1.170 α-Fe (210)
1.009	...	1.011	1.013	1.012	1.013	1.013 α-Fe (220)
Missing	...	0.905	0.906	0.905	0.906	0.906 α-Fe (310)

[a] The "best fit" values are observed for bcc α-Fe with $a = 2.8664$ Å and body centered tetragonal Fe_3B with $a = 9.63$ Å and $c = 4.29$ Å.[10]

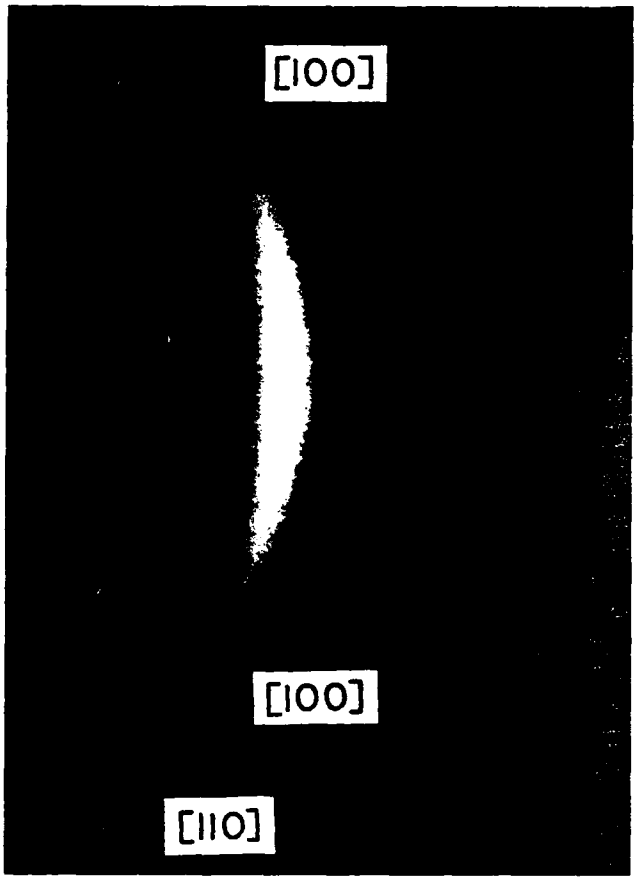

FIG. 2. Read camera photograph of the substrate wheel side of "as-quenched" Metglas 2605 CO showing the [100] and [110] fiber texture arcs on the α-Fe (110) ring which, in turn is superimposed on a broad band that originates from the amorphous regions. [The (200), (220), (211), and (311) α-Fe rings, although faintly visible in the original film, are not photographically reproducible.]

present study and the strong reflections observed for bct Fe_3B is also provided in Table I. It is possible that the absence of a reflection corresponding to the (411) plane of bct Fe_3B is due to preferred orientation. However, the amount of material corresponding to this additional phase is too small to be detected in the Read camera photographs, and we cannot make a positive identification of its structure. It is suggested that the weak diffractometer peaks are due to some kind of boride phase, and the source of the four weak peaks is referred to as the "boride phase" in what follows. We note that the four peaks associated with this phase occur only for the dull sides of the as quenched, annealed and crystalline ribbons (see Table I).

In order to test the importance of the surface crystalline layer on the magnetomechanical properties of 2605 CO Metglas, the as-quenched ribbon was given the appropriate magnetic annealing treatment to produce a high k_{33} (similar to the annealed sample) after the surface crystallinity was removed with a metallography polishing wheel. The same high value of k_{33} resulted (see Ref. 1 for experimental details), thus leading to the conclusion that the surface crystallinity layer has no effect on the ability to produce a high magnetomechanical coupling factor. On the other hand, x-ray diffractometer scans of a ribbon for which the surface crystallinity was removed and then subjected to the high k_{33} annealing treatment did show evidence of small amounts of crystallinity throughout the sample. (A previous characterization of these samples using another diffractometer which utilized molybdenum radiation without a monochromator detected no crystallinity.[1]) Overnight exposure with the Read camera of this annealed sample confirmed the presence of α-iron crystallites. Thus, although the surface crystallinity of the as-quenched sample seems to have no effect on the attainable k_{33}, there are small amounts of α-iron precipitated in high k_{33} samples by the annealing process. Upon annealing at 427 °C to produce the samples denoted as crystalline, extensive α-iron crystallization is observed and the value of k_{33} drops drastically. The shiny side of the crystalline sample, or the side without the initial surface crystallinity, shows α-iron peaks in the intensity ratio corresponding to random crystallites, while the dull side of an unpolished sample annealed at 427 °C maintains considerable preferred orientation.

To conclude the present section, two other studies conducted on the as-quenched ribbon are discussed. These experiments are the microprobe analysis and the investigation of changes in surface crystallinity with depth. Figure 3 shows a micrograph of the dull side of the as-quenched ribbon. The presence of a "peak and valley" structure is clearly evident. The surfaces were measured with a profilometer and the depth of the deepest valleys was estimated to be 2–3 μm. The intensity of the cobalt, iron and boron K_α lines was measured as the microprobe beam was laterally scanned. There was no variation detected in elemental concentration between the peak and valley regions. It should be noted that the depth of the boron sampled in the microprobe experiment is limited, not by the penetration depth of the exciting electrons, but by the absorption length of boron K_α x rays, which are reduced in intensity by a factor of $1/e$ upon passing through ≈ 40 Å of the sample. Finally, the surface of the dull side of the as-quenched sample was progressively removed with a polishing wheel, and it was observed that the x-ray diffraction peaks from the α-iron phase decreased in in-

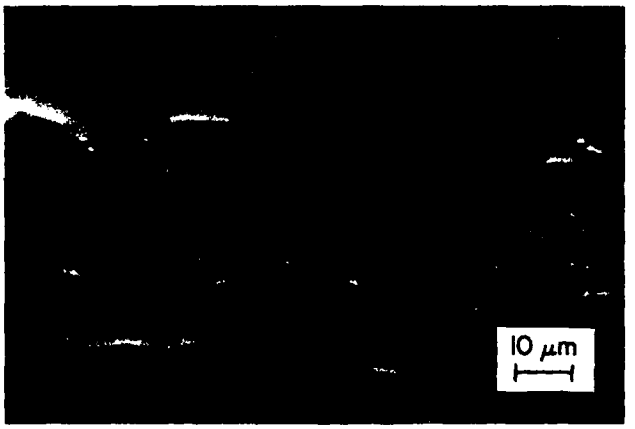

FIG. 3. Micrograph of the substrate wheel side of as-quenched Metglas 2605 CO showing the "peak and valley" texture.

tensity faster than did the peaks of the boride phase. In addition, the intensity of the α-iron (110) peak decreased more rapidly than did that of the (100) peak. All traces of surface crystallinity disappeared when $\approx 3\,\mu$m of the sample was polished away.

A crystalline surface layer, which extends into the sample $\lesssim 3\,\mu$m (as measured from the tops of the peaks), is reported for the substrate wheel (or dull) side of Metglas 2605 CO. The crystallites, an α-iron phase, are oriented in a fiber texture configuration. The fiber axis is a mixture of the [100] and [110] directions, and points along a line normal to the ribbon surface. In addition to the α-iron phase, there are small amounts of an additional crystalline phase. The additional phase is probably an iron-cobalt boride with a strong preferred orientation, but we are not able to make a definite determination of its structure.

If Metglas 2605 CO is given the appropriate magnetic annealing treatment for maximizing the magnetomechanical coupling coefficient k_{33}, the same high value of k_{33} results whether or not the surface crystallinity was removed prior to the anneal. However, such an annealing treatment produces a small amount of α-iron crystallites in the bulk. The previous spin-echo NMR experiments, which were sensitive to signals from boron and cobalt nuclei, detected no significant difference between the as-quenched and annealed samples.[2] Consistent with the predictions of Graham and Egami,[11] it was concluded that any atomic rearrangement which occurs during the magnetic annealing must involve a relatively small number of atoms, or be so subtle, that no significant change occurs in the broad NMR spectra obtained from such amorphous materials.

From the diffractometer scans, it was observed that the broad amorphous peak which is characteristic of the shiny side of the as-quenched ribbon still exists on the dull side with essentially the same intensity. The center of this peak occurs at a Bragg angle in the region of the (110) α-iron reflection. Thus, the crystalline layer must not be so thick and/or extensive in area as to significantly inhibit the observed diffraction of x rays from the amorphous material. Using the usual formula for the effective sampling depth of an x-ray diffraction peak, one can show that under the present experimental conditions, 50% of the x-ray intensity reflected into the angular region of the (110) α-iron peak comes from the top 0.55 μm. Since the amorphous peak is not strongly attenuated, significant amounts of the amorphous material must lie as close as 0.55 μm to the surface. Progressive removal of the surface by polishing systematically reduces the intensity of the crystalline peaks, however, we note that the peaks do exist to a depth of $\approx 3\,\mu$m. The description of the surface crystallinity is complicated by the profilometer result which indicates a surface texture with variations in depth of 2–3 μm. At this point, it is not clear whether the surface crystallinity is confined to certain localized regions embedded in an amorphous matrix or exists as a thin carpeting which covers the hills and valleys of the surface topology.

Finally, the suggestion is made that the boron oxidation mechanism suggested by Davis *et al.*[7] as an explanation for surface crystallinity in 2605 S does not account for surface crystallinity now observed in our 2605 CO. Although we were unable to obtain a depth profile for boron, microprobe analysis shows no significant difference in boron concentration between the peak and valley regions, at least within the outer 50–100 Å of the surface. This fact would seem to argue against the crystallinity being limited to the valleys only, and being due strictly to boron depletion in the valley regions. Furthermore, if B oxidation were to be an important mechanism, it would have to explain the observed fiber texture.

The authors wish to thank J. H. Groeger for performing the scanning electron microprobe analysis. We are also grateful to Dr. F. A. Otter for several interesting discussions which have stimulated further investigations into this area.

[1] C. Modzelewski, H. T. Savage, L. T. Kabacoff, and A. E. Clark, IEEE Trans. Magn. **MAG-17**, 2837 (1981).
[2] J. C. Ford, W. A. Hines, J. I. Budnick, A. Paoluzi, D. M. Pease, L. T. Kabacoff, and C.U. Modzelewski, J. Appl. Phys. **53**, 2288 (1982).
[3] A. S. Schaafsma, H. Snyders, F. van der Woude, J. W. Dryver, and S. Radelaar, Phys. Rev. B **20**, 4423 (1979).
[4] J. C. Swartz, R. Kossowsky, J. J. Haugh, and R. F. Krause, J. Appl. Phys. **52**, 3324 (1981).
[5] H. N. Ok and A. H. Morrish, J. Phys. F **11**, 1495 (1981).
[6] H. N. Ok and A. H. Morrish, J. Appl. Phys. **52**, 1853 (1981).
[7] L. A. Davis, N. DeCristofaro, and C. H. Smith, Proceedings of the Conference on Metallic Glasses: Science and Technology, Budapest, Hungary, 1980.
[8] Metglas is a registered trademark of the Allied Corporation.
[9] J. S. Kasper and K. Lonsdale, eds., *International Tables for X-ray Crystallography, Volume II* (Kynock, Birmingham, England, 1967), p. 167.
[10] J. L. Walter, S. F. Bartram, and R. R. Russell, Met. Trans. **9A**, 803 (1978).
[11] C. D. Graham and T. Egami, Ann. Rev. Mater. Sci. **8**, 423 (1978).

NMR and magnetic susceptibility study of the $Ca_{100-x}Al_x$ metallic glass system[a)]

W. A. Hines, P. Miller, and A. Paoluzi

University of Connecticut, Storrs, Connecticut 06268

C. L. Tsai and B. C. Giessen

Northeastern University, Boston, Massachusetts 02115

In order to investigate the atomic and electronic structures of the melt spun metallic glass system $Ca_{100-x}Al_x$ ($15 \leq x \leq 45$ at. %), measurements of the ^{27}Al NMR Knight shift and linewidth, as well as the magnetic susceptibility, have been carried out at room temperature. Spectra have been obtained for resonance frequencies ranging from 9 to 20 MHz and are characteristic of a convolution of a symmetric nuclear dipole-dipole line and an asymmetric second order quadrupole line. Both the Knight shift and linewidth remain constant throughout the entire glassy regime providing evidence for some form of short range order in this system. An analysis of the magnetic susceptibility results indicates that estimates based on the free electron model are inadequate.

PACS numbers: 76.60.Cq, 75.20.En, 71.25.Mg, 61.16.Hn

I. INTRODUCTION

During the past decade, metallic glasses, or amorphous metallic alloys, have received considerable attention from both basic and applied researchers [1]. For the most part, the research work has concerned metallic glasses of the transition metal + metalloid family. Until very recently, there existed no investigation of metallic glasses containing Group IIA metals. The first such glass was prepared independently by Giessen, et al. [2] at Northeastern University and Matyja, et al. [2] at the Technical University of Warsaw. Since that time, it has been demonstrated that Ca is a profuse glass former, and detailed studies of the thermal, mechanical and electrical properties of several Ca-based binary and ternary metallic glasses have been carried out [3,4,5]. This paper reports measurements of the nuclear magnetic resonance (NMR) Knight shift and linewidth, as well as the magnetic susceptibility, which were made on the binary Ca-Al metallic glass system. Ca-Al was selected because it consists of only two "simple" metals (i.e., electrons possessing s- and p-character) with a valence difference of one. Such a situation is ideally suited for investigating models and theories concerning the electronic structure in disordered metallic systems. Furthermore, we note that both solid Ca and Al exist in a (close-packed) fcc structure with a significant difference in atomic volume. In addition, the ^{27}Al nucleus has a favorable NMR signal and a quadrupole moment which is useful for probing the near neighbor atomic environment.

II. EXPERIMENTAL

In this work, NMR and magnetic susceptibility experiments were carried out on seven compositions of the binary $Ca_{100-x}Al_x$ metallic glass, where $15 \leq x \leq 45$ at. %. The samples were prepared on three different occasions with the following compositions: batch #1 with $x = 35$; batch #2 with $x = 20$ and 30; and batch #3 with $x = 15$, 25, 35 and 45. In all cases, arc melted alloys were spun, a process involving rapid quenching from the liquid state and which is described in detail elsewhere [6]. This technique utilizes an inside-of-the-drum, vacuum melt-spinner with silica crucibles and short melting times. The amorphous ribbons that resulted were approximately 2 mm wide and 25 μm thick, and were all checked by x-ray diffraction to verify their glassy structure. Selected samples were subjected to thermal analysis by a differential scanning calorimeter. In order to obtain a good filling factor for the NMR experiments, the ribbons were cut and stacked with alternate layers of 12 μm mylar.

All NMR spectra were obtained at room temperature for frequencies from 9 to 20 MHz by utilizing a continuous wave marginal oscillator spectrometer [7]. Incorporating the spectrometer with the usual phase sensitive detection technique yielded derivatives of the absorption curves. The magnetic field sweep was calibrated by monitoring the ^2D resonance with a separate NMR spectrometer ($\gamma = 0.653566$ kHz/Oe) [8]. In order to calculate the ^{27}Al Knight shift, a value of $\gamma = 1.1094$ kHz/Oe was used for the salt reference [8].

All measurements of the magnetic susceptibility were carried out at room temperature with a PAR model 155 vibrating sample magnetometer which was calibrated against the known saturation magnetization for Ni (room temperature value of 55.01 emu/gm). For all of the samples, plots of the bulk magnetization (per mole of the formula unit) versus magnetic field (up to 20 kOe) yielded straight lines that passed close to the origin indicating no significant ferromagnetic contamination. Values of the magnetic susceptibility were calculated from the corresponding slopes.

III. RESULTS AND ANALYSIS

Fig. 1 shows a typical NMR spectrum for ^{27}Al in these samples. The lineshapes demonstrated some asymmetry in that the high field side was broader (intensity shifted into the high field tail). A consideration of the total signal intensity indicates that the line is due to the central component only, or $+1/2 \longleftrightarrow -1/2$ transition, with the other transitions being far removed from the line due to the first order quadrupole

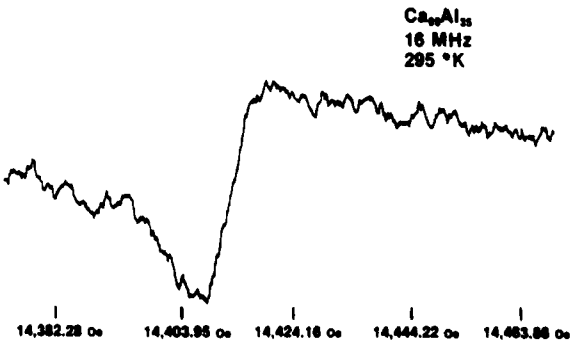

Fig. 1. Room temperature ^{27}Al NMR absorption derivative at 16 MHz for the $Ca_{65}Al_{35}$ metallic glass.

 0021-8979/82/117789-03$02.40

interaction. A consideration of the shape indicates that the line is a convolution of a symmetric gaussian form (due to the nuclear dipole-dipole interaction) and the asymmetric form which is characteristic of the second order quadrupole interaction (with some distribution in the electric field gradient) [9]. To verify the existence of the second order quadrupole interaction, ^{27}Al NMR spectra were observed as a function of resonance frequency for the $Ca_{65}Al_{35}$ sample. As the frequency was increased, intensity moved in toward the center from the tails. The linewidth (as measured from the derivative peak-to-peak) decreased from 15.3 Oe at 9 MHz to 12.5 Oe at 20 MHz, or by about 18%. This behavior is consistent with a second order quadrupole interaction which is comparable to, or perhaps smaller than, the nuclear dipole-dipole interaction. We do note that the ^{27}Al Knight shift (as measured by the derivative crossover point) was essentially independent of frequency.

Fig. 2 shows the observed ^{27}Al Knight shift as a function of the Al concentration for the Ca-Al metallic glass system. The data shown were taken at 12 MHz. Also, the values for solid Al and liquid Al (at the melting point) are indicated [9]. We note that the ^{27}Al Knight shift remains unchanged within the error over the entire range of Al concentration ($15 \leq x \leq 45$) and is about 25% that of solid or liquid Al. This is striking in that a change in the Al concentration would vary the average number of electrons per atom.

Fig. 3 shows the observed ^{27}Al linewidth as a function of the Al concentration for the Ca-Al metallic glass system. Again, the value for solid Al is indicated [9]. As is the case for the Knight shift, the linewidth remains unchanged within the error over the entire range of Al concentration. This too is striking in that substituting smaller Al atoms for the Ca atoms should change the electric field gradient and, therefore, the quadrupole interaction.

Fig. 4 shows the observed magnetic susceptibility as a function of the Al concentration for the Ca-Al metallic glass system. The measured susceptibility values have been corrected for the diamagnetism of the cores. The core contribution was obtained by taking a weighted average of Selwood's [10] values, i.e., -0.2×10^{-5} emu/mole and -0.8×10^{-5} emu/mole for Al^{+3} and Ca^{+2}, respectively. Also, the corrected values for solid Ca, solid Al and liquid Al (at the melting point) are included [10].

Following the customary analysis for simple metals, the total magnetic susceptibility, χ, can be expressed in terms of its contributions

$$\chi = \chi_{sp} + \chi_L + \chi_{core}, \qquad \text{eqn. (1)}$$

where χ_{sp} is the (Pauli) paramagnetic spin susceptibility of the conduction electrons, χ_L is the (Landau) orbital diamagnetic susceptibility of the conduction electrons and χ_{core} is the diamagnetic susceptibility of the cores. χ_{sp} can be calculated by treating the conduction (s- and p-) electrons as free with an effective mass $m^* = m$, the electron mass, and using the Pauli form (in emu/mole)

$$\chi_{sp} = (1.33 \times 10^{-6})(V_a)^{2/3}(n_{sp})^{1/3}, \qquad \text{eqn. (2)}$$

where V_a is the atomic volume in $Å^3$ and n_{sp} is the number of conduction electrons per atom. χ_L is assumed to have the Landau form

$$\chi_L = -(1/3)(m/m^*)^2\chi_{sp}, \qquad \text{eqn. (3)}$$

which becomes $-(1/3)\chi_{sp}$ when $m = m^*$ and hence, $\chi - \chi_{core} = (2/3)\chi_{sp}$. In view of the absence of a band structure and the spherical shape of the Fermi surface in the amorphous metal, taking $m = m^*$ seems reasonable. An analysis of the contributions to the magnetic susceptibility (in 10^{-5} emu/mole) is provided in Table I. For the Ca-Al metallic glass system, values for the average atomic volume, $\bar{V}_a$, were obtained from measurements of the density by Hong [3], while values for the electronic concentration, n_{sp}, were obtained from measurements of the Hall effect by Tsai, et al. [4]. A comparison of $\chi - \chi_{core}$ (column five) with $(2/3)\chi_{sp}$ (column nine) clearly shows that the simple free electron treatment of the susceptibility (spin and orbital) for the conduction electrons is small by a factor of two or three.

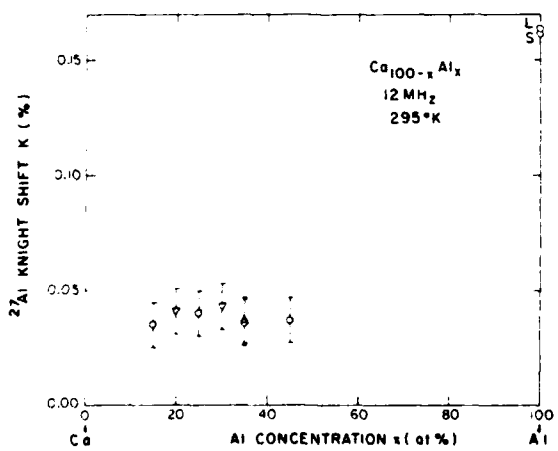

Fig. 2. Room temperature ^{27}Al NMR Knight shift at 12 MHz (in %), K, versus Al concentration (in at. %), x, for the $Ca_{100-x}Al_x$ metallic glass system: upright triangles - batch #1, inverted triangles - batch #2, circles - batch #3.

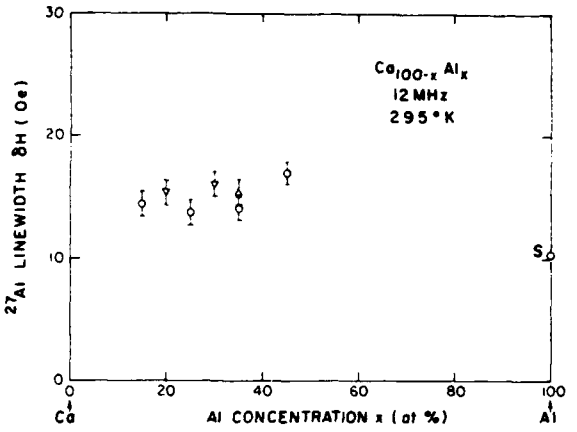

Fig. 3. Room temperature ^{27}Al NMR linewidth at 12 MHz (in Oe), δH, versus Al concentration (in at. %), x, for the $Ca_{100-x}Al_x$ metallic glass system: upright triangles - batch #1, inverted triangles - batch #2, circles - batch #3.

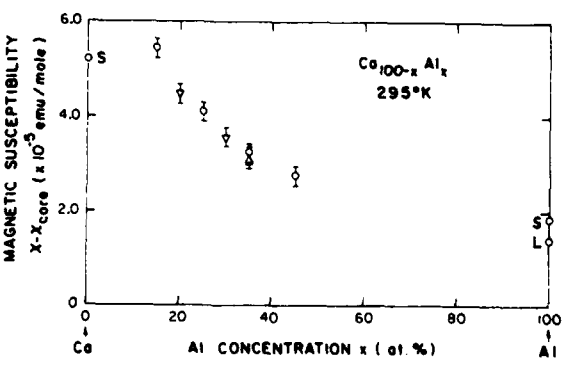

Fig. 4. Room temperature magnetic susceptibility corrected for core dramagnetism (in emu/mole), $\chi - \chi_{core}$, versus Al concentration (in at. %), x, for the $Ca_{100-x}Al_x$ metallic glass system: upright triangles - batch #1, inverted triangles - batch #2, circles - batch #3.

Table I

Measured, calculated and derived magnetic susceptibilities (in 10^{-5} emu/mole) at room temperature

Metal or alloy (batch)	State and structure	χ (measured)	χ_{core} (Selwood[10])	$\chi - \chi_{core}$ (derived)	$\bar{V}_a$ ($\AA^3$) (Hong [3])	n_{sp}(electrons/atom) (Tsai, et al.[4])	χ_{sp} (Pauli)	$(2/3)\chi_{sp}$ (Landau)
Ca	solid, fcc	4.40	-0.80	5.20	43.49	(2.0)	2.07	1.38
$Ca_{85}Al_{15}$ (3)	solid, amor.	4.73	-0.71	5.44	37.42	2.4	1.99	1.33
$Ca_{80}Al_{20}$ (2)	solid, amor.	3.78	-0.68	4.46	36.24	2.1	1.86	1.24
$Ca_{75}Al_{25}$ (3)	solid, amor.	3.46	-0.65	4.11	34.50	1.9	1.74	1.16
$Ca_{70}Al_{30}$ (2)	solid, amor.	2.94	-0.62	3.56	32.82	1.8	1.66	1.11
$Ca_{65}Al_{35}$ (1)	solid, amor.	2.50	-0.59	3.09	31.22	1.7	1.57	1.05
$Ca_{65}Al_{35}$ (3)	solid, amor.	2.64	-0.59	3.23	31.22	1.7	1.57	1.05
$Ca_{55}Al_{45}$ (3)	solid, amor.	2.21	-0.53	2.74	28.22	1.6	1.44	0.96
Al	solid, fcc	1.65	-0.20	1.85	16.60	(3.0)	1.24	0.83
Al	liquid	1.20	-0.20	1.40	18.81	(3.0)	1.35	0.90

We note, however, that this treatment neglects electron-electron interactions (correlation). A discussion of all the NMR and susceptibility results is provided in Section IV.

IV. DISCUSSION AND CONCLUSIONS

The most significant result from this study of the binary $Ca_{100-x}Al_x$ metallic glass system is that both the ^{27}Al Knight shift and linewidth remain unchanged within the error throughout the entire range of composition ($15 \leq x \leq 45$). This occurs in spite of the fact that both the average electronic concentration and the average atomic volume change appreciably. In contrast, we note that for several transition metal + metalloid systems, the metalloid Knight shift decreases dramatically as the metalloid concentration, and hence the electronic concentration, is increased (see Fig. 1, ref. 11). Also, for the same transition metal + metalloid systems, the linewidth is very sensitive to composition [12]. This result provides evidence that certain features of the nearest neighbor atomic environment and the electronic structure remain fixed as the composition is varied within the glassy regime (i.e., some form of short range order). We note that from her studies of the heat of mixing and average atomic volume, Hong [3] concludes that strong interactions exist between constituent elements in Ca-Al. Furthermore, the ^{27}Al linewidth narrows somewhat with increasing resonance frequency in the Ca-Al metallic glasses and possesses a shape that is a convolution of a symmetrical nuclear dipole-dipole line and an asymmetric second order quadrupole line. In contrast, all of the metalloid linewidths in the transition metal + metalloid systems increase with frequency in a manner characteristic of a broadening mechanism resulting from a distribution of Knight shifts, i.e., an inhomogeneity in the electronic structure [12]. This was attributed to the metalloid atoms having a variety of environments in the glassy structure. We do note, however, that the (constant) ^{27}Al Knight shift in Ca-Al is quite small (+0.038%) compared to the ^{31}P Knight shift in the Ni-Pd-P, Ni-Pt-P and Ni-P systems (ranges from +0.160% to +0.260%) [11].

Finally, an estimate of the conduction electron contribution to the magnetic susceptibility for Ca-Al (both spin and orbital) assuming the free electron model with the customary Pauli and Landau forms yields values which are too small by factors of two to three. This discrepancy probably arises, for the most part, from the omission of electron-electron interactions (correlation). Such effects are known to account for factors of two in the most simple metals (i.e., Li and Na). In any case, an inspection of the values in Table I seems to indicate that the decreases in $\bar{V}_a$ and n_{sp} are not enough to account for the observed decrease in $\chi - \chi_{core}$. The values for n_{sp} were taken from Hall effect experiments [4]. Using weighted averages of the Ca and Al valence (two and three, respectively) for n_{sp} makes the situation worse in that the trend is wrong. Making estimates for the electron-electron interaction by taking weighted averages from the solid Ca and Al data helps considerably. However, as pointed out by Tsai, et al. [4], the existence of low lying d-states in Ca will affect the electronic structure and, consequently, Ca-base metallic glasses with electron-richer addition elements may show a behavior more complicated than a simple free electron picture. In order to gain additional insight into the nature of the electronic density of states for this system, heat capacity experiments have just been initiated.

REFERENCES

a) Work at University of Connecticut supported by the AFOSR (80-0030) and Northeastern University by the NSF (DMR 77-23777).

[1] Glassy Metals I, edited by H. -J. Güntherodt and H. Beck (Springer-Verlag, New York, 1981).

[2] A. Calka, M. Madhava, D. E. Polk, B. C. Giessen, H. Matyja and J. Vander Sande, Scripta Met. 11, 65 (1977).

[3] J. Hong, Ph.D. thesis, Northeastern University (1979).

[4] C. L. Tsai, J. Hong and B. C. Giessen, to be published in Rapidly Quenched Metals IV (1982).

[5] J. P. Carini, S. Basak, S. R. Nagel, B. C. Giessen and C. L. Tsai, Phys. Letters 81A, 525 (1981).

[6] R. Pond and R. Maddin, Trans. Met. Soc. AIME 245, 2475 (1969).

[7] R. V. Pound and W. D. Knight, Rev. Sci. Instrum. 21, 219 (1950).

[8] Varian Associates, NMR Chart of the Nuclei.

[9] L. E. Drain, Metall. Rev. 12, 195 (1967).

[10] P. W. Selwood, Magnetochemistry (Interscience, New York, 1956).

[11] W. A. Hines, C. U. Modzelewski, R. N. Paolino and R. Hasegawa, Solid State Commun. 39, 699 (1981).

[12] W. A. Hines, L. T. Kabacoff, R. Hasegawa and P. Duwez, J. Appl. Phys. 49, 1724 (1978).

Magnetic properties of some new Co–Nb–B metallic glasses

R. C. O'Handley, B. W. Corb, Y. Hara, and N. J. Grant

Massachusetts Institute of Technology, Cambridge, Massachusetts

W. Hines

University of Connecticut, Storrs, Connecticut 06268

Several new amorphous metallic alloys based on cobalt or iron and stabilized with up to 10 at.% boron and up to 14 at.% niobium have been melt spun to ribbon form. Notable are $Co_{80}Nb_{14}B_6$, $Co_{84}Nb_{10}B_6$, and $Fe_{81}Nb_5B_{14}$. The cobalt moment and Curie temperature reductions due to niobium are stronger than those due to boron. These new glasses show attractive soft ferromagnetic properties—similar to those of the familiar transition metal/metalloid glasses—while offering improved thermal stability despite the reduced metalloid content.

PACS numbers: 75.50.Kj, 75.60. – d

INTRODUCTION

Of the variety of classes of amorphous metallic alloys investigated in recent years, the most promising from a technological point of view have been the late transition metal/metalloid variety, typically $TL_{100-x}M_x$ (TL = Fe, Co, Ni..., M = B, C, Si, P..., and $15 < x < 25$ at%). However, the presence of the metalloid – necessary for glass formation and stability – significantly lowers the magnetic moment relative to that of the pure TL species and more recently has been associated with the existence of crystal nuclei of a brittle TL–M phase that can degrade soft magnetic properties [1].

The present work was motivated by the desire to study the effects of early transition metal (TE) substitutions on the TL moment and at the same time exploit the strong TE–TL bonding as a means of lowering the metalloid content. Any microcrystalline nuclei present in such low-metalloid alloys would probably be of a primary solid solution of TE in α-TL. Moreover, upon intentional crystallization such alloys would be likely to retain the ductility characteristic of their glassy state. Cobalt-base rather than iron-base glasses have been examined first in detail because of their low magnetostriction and the existence of several favorable eutectics with TE species [2].

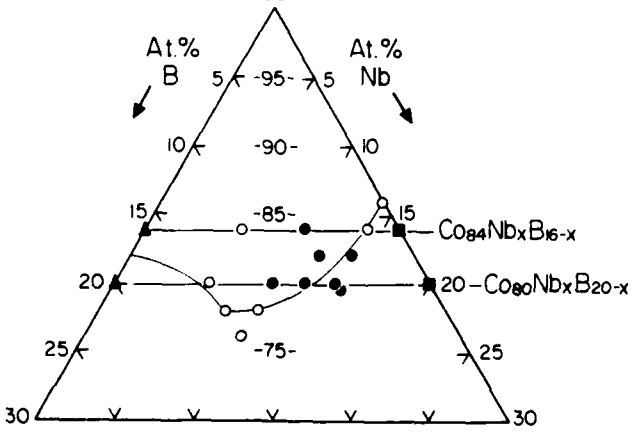

Fig. 1 Cobalt-rich corner of Co–Nb–B diagram showing fields of primary crystallization products (Ref. 3). Closed circles indicate compositions melt spun to glassy ribbons and open circles those melt spun to microcrystalline ribbons. Triangles and squares represent data for glassy compositions from literature: CoB [5] and CoNb [6].

RESULTS

Magnetization

Fig. 1 shows the path of the equilibrium ternary eutectic in the Co–Nb–B system [3] and indicates compositions that we have melt-spun to the glassy (closed circles) and crystalline (open circles) states. The range of alloys we studied is less extensive and shows a smaller glass-forming region than that reported by Ohnuma et al [4]. Data for the one Fe-base glass made are included for comparison. The compositions and room temperature magnetizations of the alloys from Fig. 1 are listed in Table I. Data for two sets of alloys $Co_aNb_xB_{100-a-x}$ (a = 80 and 84 at%) which cut across Fig. 1 on constant cobalt lines are shown in Fig. 2. Literature values have been used for the end member magnetizations: $Co_{100-x}B_x$ glassy ribbons [5] and $Co_{100-x}Nb_x$ amorphous sputtered thin films [6]. The discrepancy between the trend in the glassy ribbon data and the thin film values is discussed below.

TABLE I

Composition (at%) Co	Nb	B	σ(295) (emu/g)	T_c (K)	atomic structure glassy	crystalline
79.6	14.7	5.7	67.3		x	
80	14	6	73.6	825	x	
80	12	8	83.5		x	
80	10	10	89		x	
80	6	14	106.3			x
84	10	6	96	1023	x	
84	14	2	61.1			x
84	6	10	112.5			x
86	14		65.1			x
82	12	6	88.5		x	
78	8	14	99			x
78	10	12	69.8			x
76	10	14	62			x
82	14	4	61.4		x	
$Fe_{81}Nb_5B_{14}$			106	407	x	

Technical properties

Table II lists (Curie temperatures and) some technical properties of two of the Co-base glasses and, for comparison, those for the Fe-base glass. These new glasses are seen to be more stable than typical TL–B glasses [2] for which $T_x = 650$K. Saturation magnetizations (295K) are lowered more by Nb than by

 0021-8979/82/117753-03$02.40

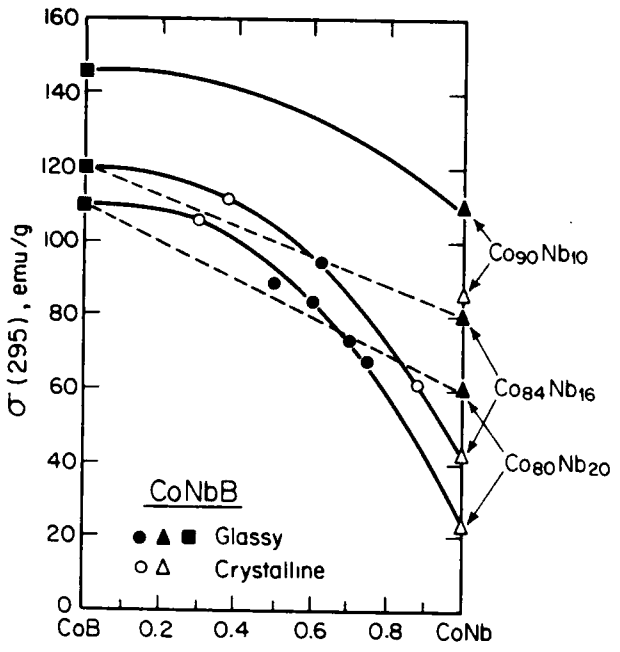

Fig. 2 Room temperature specific saturation magnetizations for those samples of Fig. 1 that lie along the two lines of constant cobalt concentration. For crystalline cobalt σ(295K) = 160 emu/g. Values for σ(295) for recrystallized CoNb films have been included as open triangles to aid in the interpretation of the ternary alloy results.

boron substitutions because of increased saturation moment reduction and Curie temperature suppression. These effects are offset somewhat by the increased mass density of Nb-containing glasses relative to Co-B glasses. The as-cast coercivities are attractive but the failure to observe a B-H loop in the Co_{84} glass (its Mo-K_α diffraction pattern was equally as smooth and free of any sign of crystallinity as was that of the Co_{80} glass) prompted a study of the magnetic domains.

TABLE II

Composition (at%)	σ(295K) (emu/g)	Density (g/cm^3)	$4\pi M_s$ (kG)	T_C (K)	H_c (mOe)
$Co_{80}Nb_{14}B_6$	73.6	8.6	7.96	825	30
$Co_{84}Nb_{10}B_6$	96	8.45	10.2	1023	-
$Fe_{81}Nb_5B_{14}$	106	7.2	9.6	407	50

Domains

Fig. 3 shows the domain patterns observed using a Bitter solution [7] on unpolished ribbons held in an in-plane field of 10 Oe. The maze-domain pattern extends over the entire sample surface in $Co_{84}Nb_{10}B_6$ glass. Clearly the absence of a loop in this glass is due to a perpendicular anisotropy which stabilizes the domain pattern. In perpendicular fields of 10 Oe, maze domain patterns were only observed in isolated patches of the $Co_{80}Nb_{14}B_6$ ribbon.

DISCUSSION

Magnetizations

Fig. 2 indicates a steeper magnetization suppression with Nb content than with B content. The component of this due to moment suppression is given by

$$\partial\mu_{Co}/\partial c_B = -3\ \mu_B\ [5] \quad \text{and} \quad \partial\mu_{Co}/\partial c_{Nb} = -5.2\ \mu_B\ [6]$$

while the Curie temperatures of the Nb-containing glasses are also lower: $T_C(Co_{84}B_{14}) > 880K$ [5] and $T_C(Co_{83.5}Nb_{16.5}) = 800K$ [6]. The magnetic moments of CoNbB alloys are being investigated in more detail and may be interpreted in terms of split d bands. In this model Nb d states above E_F hybridize with the lower lying Co d states to an extent that depends upon the boron concentration: strong Nb-B bonding lowers the Nb d states bringing them closer in energy to those of Co and thus allowing more d-d hybridization [8].

The greater magnetization of the amorphous Co-Nb thin films relative to the trend in the glassy and crystalline melt-spun Co-Nb-B alloys (Fig. 2) requires an explanation. We speculate that a more random atomic arrangement exists in the sputtered films (giving a $Co_{1-x}Nb_x$ supersaturated solid solution) while the slower quench rate of melt spinning allows for the development of more Co-Nb short-range order possibly close to that of the stable Laves phase Co_2Nb [2,3]. The magnetization data then require:

$$\sigma(Co_{1-x}Nb_x) > x\sigma(Co_2Nb) + (1-3x)\sigma(Co)$$

This relation is in fact supported by the crystallization behavior of the thin films which show a decrease in magnetization at T_x presumably with the appearance of Co_2Nb [6] whereas the melt-spun ribbons show a magnetizaition increase at T_x.

Technical properties and domains

It is tempting to attribute the perpendicular anisotropy of the Co_{84} glass to stress. However, Naka et al [6] have shown that for $Co_{1-x}Nb_x$ amorphous thin films the magnetostriction is very small, $\lambda = -1.5 \times 10^{-6}$, (and nearly independent of x) and for $Co_{1-x}B_x$ glasses $\lambda = -4 \times 10^{-6}$ (again only weakly dependent on x) [9]. Thus $Co_{84}Nb_{10}B_6$ should have a weak negative magnetostriction comparable in magnitude to that of $Co_{80}Nb_{14}B_6$. The difference between these two glasses

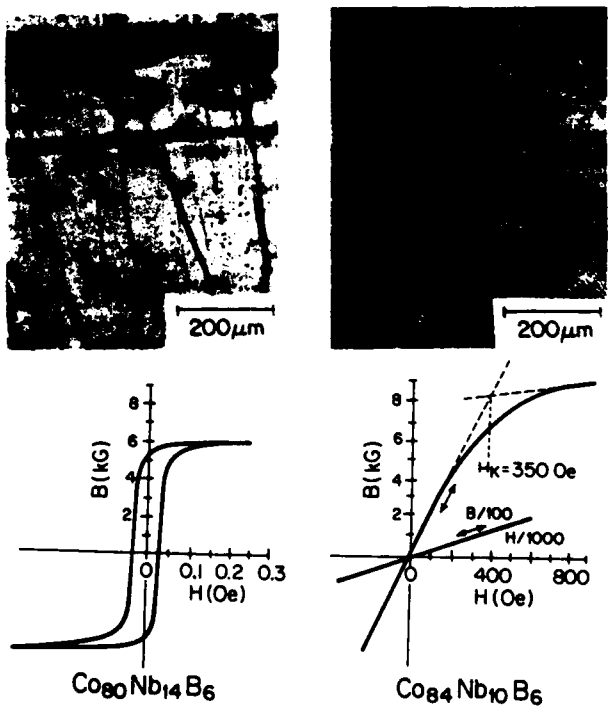

Fig. 3 Bitter solution domain patterns of $Co_{80}Nb_{14}B_6$ and $Co_{84}Nb_{10}B_6$ glassy alloys in 10 Oe in-plane field. Below each domain picture is a representative dc B-H curve. The Co_{84} glass shows no hysteresis, consistent with the out-of-plane magnetization implied by its superficial domain pattern.

may then lie in their short-range order and hence the structure of any microcrystalline nuclei which might be present in the glass. The phase diagram [3] suggests that for $Co_{84}Nb_{10}B_6$ such nuclei would more likely be of a close-packed cobalt structure whereas for $Co_{80}Nb_{14}B_6$ such nuclei would more likely be of the Laves phase Co_2Nb [10]. It is possible that a larger (though undetectable by X-ray diffraction) concentration of α-Co precipitates exists because they would exhibit faster nucleation kinetics than the complex Laves phase. The Co crystallites might be responsibly for a built-in stress field which couples through the magnetostriction to give rise to the maze-like domain pattern and B-H characteristic of Fig. 3.

SUMMARY

CoNb B glasses represent a new class of metallic glasses which exhibit interesting magnetic moment behavior due to Nb d states above the Fermi energy. They show potentially useful technical properties - low coercivity, good thermal staiblity and high magnetization. For high cobalt content, a perpendicular magnetic anisotropy exists in the as-cast glassy ribbons.

ACKNOWLEDGEMENT

We are pleased to acknowledge the support of the work at MIT by ARO contract No. DAAG-29-80-K-0088 and NSF Grant No. 78-24185 DMR and that portion at U. Conn. by AFOSR Contract No. 80-0030. We are also grateful to Dr. S. Foner for the use of his magnetometer at the outset of this work before ours was operational.

REFERENCES

[1] R. Hasegawa, G.E.Fish and V.R.V. Ramanan, PROCEEDINGS OF FOURTH INTERNATIONAL CONFERENCE ON RAPIDLY QUENCHED METALS (RQM IV), Ed. T. Masumoto and K. Suzuki (Japan. Inst. Metals, Sendai, 1982) p. 929, and A.Datta, N. DeCristofaro, and L.A. Davis, ibid. p. 1007.

[2] R.C. O'Handley and N.J. Grant, in RAPIDLY SOLIDIFIED AMORPHOUS AND CRYSTALLINE ALLOYS, ed. B. H. Kear and B. C. Giessen (Elsevier, North-Holland, NY, 1982).

[3] H.H. Stadlemaier and J.D. Schobel, METALL 20, 31 (1966).

[4] S. Ohnuma, J. Kanehira, K. Shirakawa, T. Egami and T. Masumoto in RQM IV op cit. p. 1047

[5] R. Hasegawa and R. Ray, J. Appl. Phys. 50, 1586, (1979).

[6] M. Naka, N.S.Kazama, H. Fujimori, and T. Masuomoto, in RQM IV op. cit. p. 919.

[7] Solution No. EMG-807 from Ferrofluidics Inc., Nashua, NH 03061

[8] R.C. O'Handley, B.W. Corb, N.J. Grant and V. Moruzzi, paper to be presented at ICM 82, Kyoto

[9] K. Narita, J. Yamasaki and H. Fukunaga, J. Appl. Phys. 50,7591 (1979) and J. Aboaf and E. Klokholm, J. Magn. and Mag. Mat. 15-18, 1385 (1980).

[10] The likelihood of α-Co nuclei existing in $Co_{84}Nb_{10}B_6$ glass is supported by the different crystallization temperatures detected in that composition by DSC and magnetization measurements. (For $Co_{80}Nb_{14}B_6$ both DSC and magnetization suggest rapid crystallization at 743K.) DSC shows a crystallization exotherm in the Co_{84} glass at 698K. This phase change represents nucleation of more (rapid growth of the) α-Co nuclei and has no detectable effect on the saturation magnetization. Only at T = 723K is a rapid increase in magnetization observed signalling a change in local order possibly through the growth of Co nuclei.

IV. ATOMIC AND ELECTRONIC STRUCTURES OF THE Ca-Al METALLIC GLASS SYSTEM: A PULSE NMR STUDY

A. Introduction

In spite of the considerable research effort devoted to metallic glasses during the past decade, fundamental questions concerning the atomic and electronic structures remain unanswered. Nuclear magnetic resonance (NMR) is a very powerful tool for investigating the microscopic properties of liquids, and both amorphous and crystalline solids. In particular, information concerning the atomic structure can be obtained through the electric quadrupole interaction, while the hyperfine interaction is useful for electronic structure studies. With this in mind, measurements of the NMR Knight shift and linewidth, as well as the magnetic susceptibility, were recently carried out on the binary $Ca_{100-x}Al_x$ metallic glass system for $15 \leq x \leq 45$[11]. These initial measurements were carried out at room temperature using steady state (cw) NMR techniques. All of the observed spectra were attributed to the ^{27}Al central component, or $-1/2 \longleftrightarrow +1/2$ transition, with the other transitions being far removed from the line due to the first order quadrupole interaction. The most significant observation in the early study was that both the ^{27}Al Knight shift and linewidth remain unchanged within error throughout the entire range of composition. This occurs in spite of the fact that both the average atomic volume and average electronic concentration change appreciably. The initial results seem to suggest that some form of short range order exists in this simple metal system, similar to that observed for transition metal + metalloid metallic glasses. In order to explore further the nature of any short range order, additional pulse NMR experiments have been carried out. This paper presents spin-echo measurements of the entire ^{27}Al quadrupole spectra for the $Ca_{100-x}Al_x$ metallic glass system. Spectra from the metallic

glasses are compared with similar spectra from the related crystalline compounds, Ca_3Al and $CaAl_2$. In addition, measurements of the NMR spin-lattice relaxation time, T_1, are presented which support the earlier Knight shift results.

B. Experimental Apparatus and Procedure

In this work, pulse NMR experiments were carried out on eight compositions of the binary Ca-Al metallic glass system and three related crystalline alloys. The metallic glass samples, designated a-$Ca_{100-x}Al_x$ with $15 \leq x \leq 45$ were prepared by rapid quenching from the liquid state utilizing an inside-of-the-drum, vacuum melt spinner[12]. All of the amorphous ribbons were checked by x-ray diffraction to verify their glassy structure; selected samples were subjected to thermal analysis by a differential scanning calorimeter. The related crystalline samples are designated c-Ca_3Al, c-$Ca_{55}Al_{45}$ and c-$CaAl_2$. The crystalline sample c-$CaAl_2$ was made directly in ingot form by arc melting, while c-Ca_3Al (or c-$Ca_{75}Al_{25}$) and c-$Ca_{55}Al_{45}$ were obtained by crystallizing the corresponding metallic glasses and, therefore, are in ribbon form.

The variable frequency pulsed NMR apparatus and single-coil arrangement are similar to those described elsewhere[13]. Entire quadrupolar broadened spectra were observed by using the conventional spin-echo technique, $\pi/2 - \pi$ pulse sequence, with a "boxcar" integrator and sweeping the magnetic field. Measurements of the nuclear spin-lattice relaxation time, T_1, were made by employing a $\pi/2 - \pi/2$ pulse sequence. Knight shift, K, measurements were obtained by using a single $\pi/2$ pulse and sweeping the magnetic field through the central transition with the boxcar to obtain the absorption signal by integrating the free-induction decay.

C. Results and Analysis

In this study, information concerning the atomic structure of the $Ca_{100-x}Al_x$ metallic glass system and the related crystalline phases was obtained by an NMR investigation of the interaction between the nuclear quadrupole moment of ^{27}Al and the electric field gradient which reflects its local environment. We note that NMR has been used extensively for such studies in non-metallic glasses[14]. The strength of the interaction of the electric quadrupole moment (eQ) with the electric field gradient ($eq = V_{zz}$) is described by the quadrupolar frequency, $\nu_Q = 3e^2qQ/2I(2I + 1)h$, where $I = 5/2$ for Al. A dimensionless asymmetry parameter, $\eta = |V_{xx} - V_{yy}|/|V_{zz}|$ (where $0 \leq \eta \leq 1$), measures the deviation from uniaxial symmetry.

Fig. 1 shows the ^{27}Al spin-echo NMR spectra observed at 4.2 °K and 10.5 MHz for four representative compositions from the a-$Ca_{100-x}Al_x$ metallic glass system (x = 15, 25, 35 and 45). Except for signal intensity, the spectra observed for the other intermediate compositions are similar in every respect. All of the spectra are significantly broadened by the electric quadrupole interaction and consist of a characteristic peak associated with the central transition and wings extending over 2 kOe (2 MHz) associated with all other transitions. Although the Al concentration, x, increases by a factor of three over the glassy regime and, therefore, substantial changes in the electric field gradient would be expected, the observed qualitative features of the spectra remain unchanged. The observed signal intensity simply scales with the number of resonating ^{27}Al nuclei. The spectra indicate that there is a significant distribution in the electric field gradient surrounding an Al atom and the local symmetry is non-uniaxial.

Fig. 2 shows the ^{27}Al spin-echo NMR spectra observed at 4.2 °K and 10.5 MHz for the three crystalline alloys, c-Ca_3Al, c-$Ca_{55}Al_{45}$ and c-$CaAl_2$, as well as the a-$Ca_{65}Al_{35}$ metallic glass. Only the c-$CaAl_2$ spectrum demon-

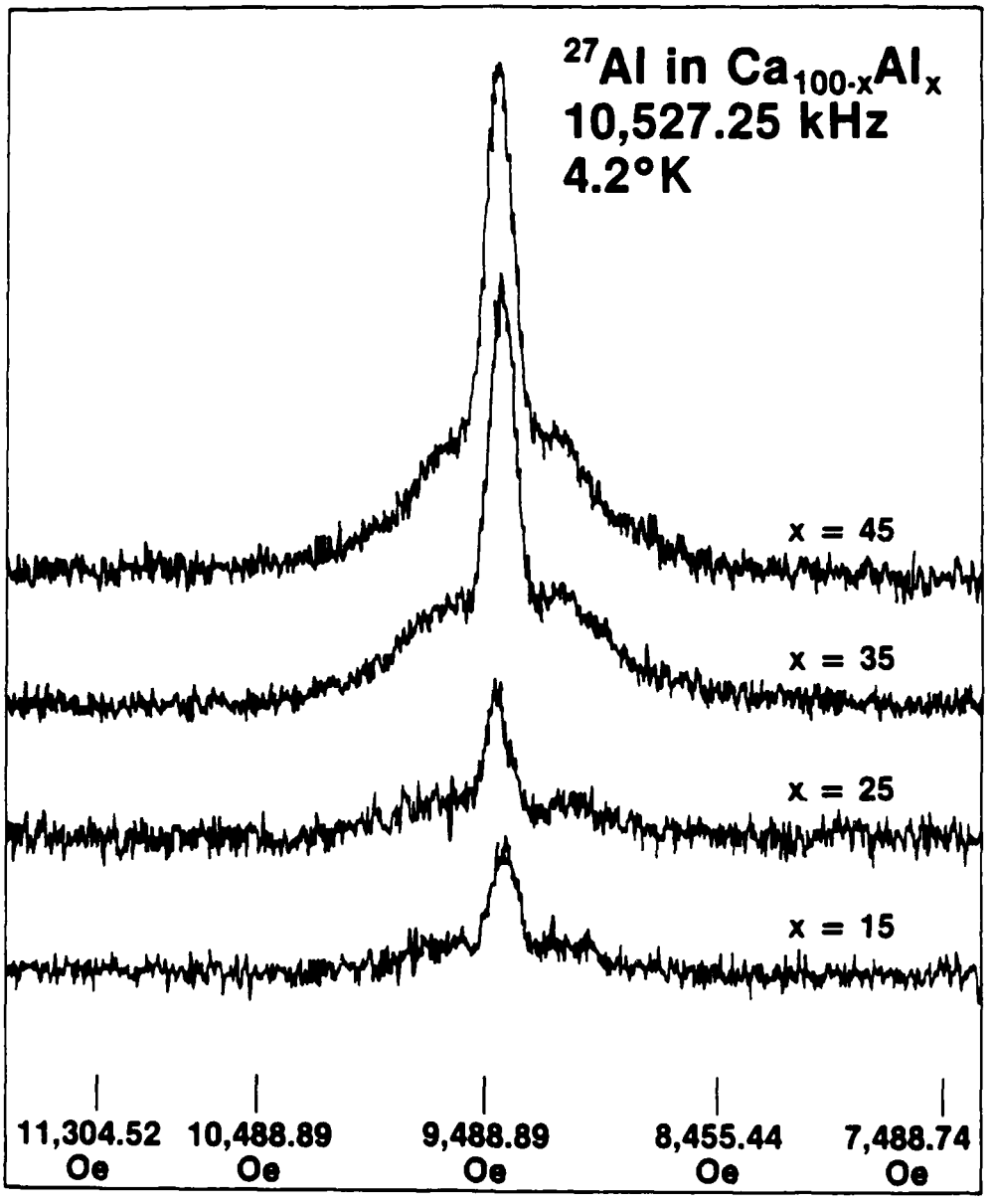

FIGURE 1
^{27}Al spin-echo quadrupole spectra
for $Ca_{100-x}Al_x$ metallic glasses

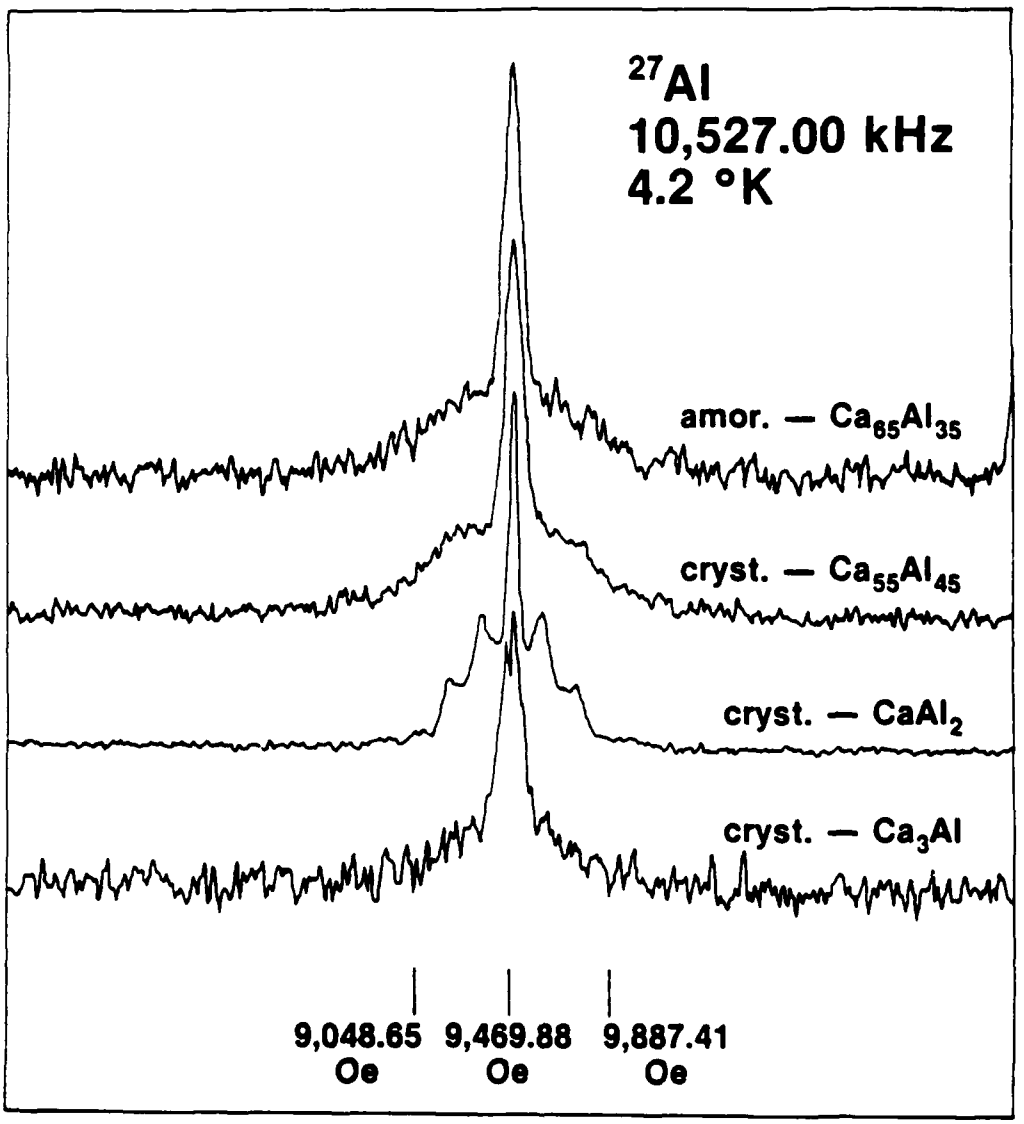

FIGURE 2
^{27}Al spin-echo quadrupole spectra
for related crystalline alloys

strates the distinct features which are characteristic of a well-ordered environment for the Al atoms. The c-$CaAl_2$ spectrum is typical of those observed for I = 5/2 nuclei in a single type of site with uniaxial symmetry (η = 0) and ν_Q = 294 kHz. There is essentially no distribution in the electric field gradient. This is expected as c-$CaAl_2$ is a member of the cubic Laves (AB_2) family; a class of compounds which crystallize with a cubic structure but possess atoms at sites of less-than-cubic symmetry. X-ray diffraction measurements on the c-$CaAl_2$ sample confirmed the Laves structure. The other two crystalline samples, c-Ca_3Al and c-$Ca_{55}Al_{45}$ demonstrate non-uniaxial symmetry for the local Al environment and considerable distribution in the electric field gradient similar to that observed for the a-$Ca_{100-x}Al_x$ metallic glasses. As of this writing, efforts based on x-ray diffraction have proved unsuccessful in identifying the c-Ca_3Al phase. c-$Ca_{55}Al_{45}$ is a two phase combination of c-Ca_3Al and c-$CaAl_2$.

Preliminary values for the spin-spin relaxation time, T_2, were obtained at 4.2 °K and 10.5 MHz in the conventional way by measuring the spin-echo amplitude as a function of the time delay between the $\pi/2$ and π pulses. As expected, the value for T_2 characteristic of the central peak is significantly shorter than the value characteristic of the wings. (For a-$Ca_{65}Al_{35}$, the values are 1.2 msec and 2.3 msec, respectively.) This fact was exploited in obtaining central peak T_2 values for selected samples (see Table I). Except for c-$Ca_{55}Al_{45}$, all of the samples demonstrated exponential behavior for the central peak echo versus time delay thereby yielding single values for T_2. c-$Ca_{55}Al_{45}$ possessed both long and short components to T_2, which are associated with Al in the two phases. T_2^* values were also obtained at 4.2 °K for selected samples from the observed free induction decay (see Table I).

TABLE I

Sample	T_2 (msec)	T_2^* (μsec)	K (%)
a-$Ca_{65}Al_{35}$	1.2	13	0.042
c-Ca_3Al	1.7	58	-0.003
c-$Ca_{55}Al_{45}$	0.39 >1.2	22	0.033
c-$CaAl_2$	0.42	17	0.107

The details of the ^{27}Al central transition spectra for the three crystalline alloys as well as the a-$Ca_{65}Al_{35}$ metallic glass were investigated by making integrated free induction decay sweeps at room temperature and 10.5 MHz. Consistent with the spin-echo spectrum described above, the central transition spectrum for c-$CaAl_2$ is a typical second order quadrupolar broadened powder pattern for a single type of site possessing uniaxial symmetry with ν_Q = 299 kHz and essentially no distribution in the electric field gradient. The other two crystalline samples, c-Ca_3Al and c-$Ca_{55}Al_{45}$ are also broadened by the second order quadrupole interaction, however, as observed in the spin-echo spectra, there is non-uniaxial symmetry and considerable distribution in the electric field gradient for both cases. The room temperature Knight shift values obtained from the central transition spectra are listed in Table I. The room temperature values of ν_Q = 299 kHz and K = 0.107% for c-$CaAl_2$ are consistent with the work of Barnes, et al.[15], while K = 0.042% for a-$Ca_{65}Al_{35}$ is consistent with the earlier work[11].

Fig. 3 shows the measured ^{27}Al nuclear spin-lattice relaxation rate as a function of the Al concentration for the a-$Ca_{100-x}Al_x$ metallic glass system. The data were taken at 4.2 °K and 10.5 MHz. Also shown is the value for pure crystalline Al. We note that the ^{27}Al relaxation rate remains unchanged within the error over the entire range of Al concentration

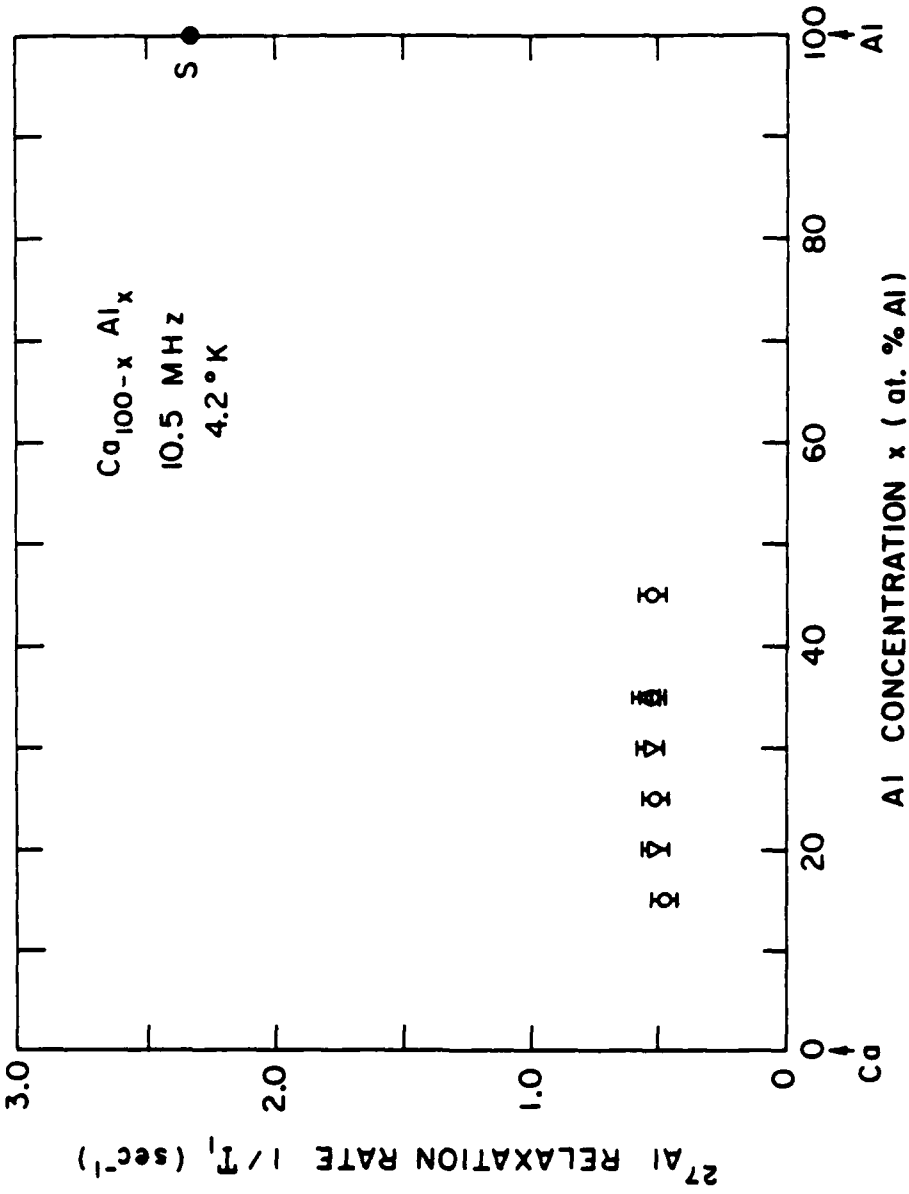

FIGURE 3
^{27}Al spin-lattice relaxation rate
for $Ca_{100-x}Al_x$ metallic glasses

($15 \leq x \leq 45$) and is about 22% that for crystalline Al. This behavior is consistent with the earlier Knight shift measurements[11], and is significant in that a change in the Al concentration would vary the average number of electrons per atom.

D. Discussion and Conclusions

This paper presents spin-echo quadrupole spectra for the $Ca_{100-x}Al_x$ metallic glass system and related crystalline compounds. To our knowledge, this is the first such observation in a simple metal system. Panissod, et al.[16] have observed the spin-echo spectra in a series of transition metal + metalloid systems: (1) ^{71}Ga in splat-cooled glassy $La_{75}Ga_{25}$, (2) ^{11}B in sputtered amorphous $Mo_{70}B_{30}$ and in splat-cooled glassy $Mo_{48}Ru_{32}B_{20}$, and (3) ^{11}B in glassy $Ni_{78}P_{14}B_8$ quenched from the melt. Their work demonstrated that, independent of the preparation technique, the electric field gradient surrounding the metalloid atoms in the amorphous alloys possessed the same local symmetry as the corresponding crystalline compounds, i.e., cubic La_3Ga, tetragonal Mo_2B and orthorhombic Ni_3B. In their analysis of the ^{11}B quadrupole spectra in $Ni_{100-x}B_x$ metallic glasses, Panissod, et al.[17] find that the symmetry of the electric field gradient for the x = 18.5 and 40.0 concentrations are similar to the compositionally closest nickel borides (Ni_3B and Ni_4B_3, respectively), and conclude that the local atomic structure is therefore similar. Furthermore, they suggest that the intermediate concentrations are related to an admixture of crystalline Ni_3B and Ni_4B_3. There is increasing evidence for the existence of short range order in the transition metal + metalloid metallic glasses. As of this writing, the situation for the $Ca_{100-x}Al_x$ simple metal system is not as definitive. It is striking that, although the Al concentration varies by a factor of three, the qualitative features of the spectra remain unchanged throughout the entire glassy regime. The observed quadrupole spectra for the metallic

glasses indicate that there is considerable distribution in the electric field gradient surrounding an Al atom and the local symmetry is non-uniaxial. This is also the case for the compositionally closest phase, Ca_3Al, which is not identified at this time. However, significant differences in the spectra and spin-spin relaxation times exist between the $Ca_{100-x}Al_x$ metallic glasses and Ca_3Al.

Finally, the experimental results indicate that the Knight shift ($K = 0.038\% \pm 0.010\%$ at room temperature) measured in the earlier work[11], and spin-lattice relaxation time ($T_1 = 2.0 \pm 0.2$ sec) measured in this work remain constant throughout the entire glassy regime. In addition, the small value for K, and correspondingly the long spin-lattice relaxation time, indicates that the local density of s-electron states at the Al sites is small. These results are consistent with recent ultraviolet photoemission spectroscopy experiments by Nagel, et al.[18] Furthermore, Nagel, et al.[18] have done augmented-spherical-wave band structure calculations for Ca_3Al and CaAl in various crystal structures. In particular, the calculated s-electron density of states at the Al sites is very small and flat in the vicinity of the Fermi energy. Since the Knight shift and spin-lattice relaxation rate provide a direct measure of the density of states at the Fermi energy, our results support the band structure calculations.

V. ON THE DENSITY OF UNOCCUPIED d STATES IN TRANSITION METAL + METALLOID METALLIC GLASSES

A. Introduction

In studies of the electronic structure of transition metal + metalloid (TM + G) metallic glasses, it is often found that the density of d states at the Fermi level $\rho_d(E_f)$ is sharply reduced in the glass relative to the pure transition metal. Thus, photoemission, magnetic susceptibility, and specific heat measurements indicate that $\rho_d(E_f)$ is considerably lowered in several metallic glasses based on either a Pd or Ni transition metal matrix[19,20,21,22,23]. ^{195}Pt Knight shift results for the $(Ni_yPt_{1-y})_{75}P_{25}$ system show that the large negative core polarization contribution to the Knight shift in pure Pt is not present in the metallic glasses studied[24]. In these systems, the ^{195}Pt Knight shift is nearly zero, indicating a low value of $\rho_d(E_f)$.

When a low value of $\rho_d(E_f)$ is observed in a metallic glass, it is a common practice to interpret this observation in terms of a filling of the transition metal d band. For instance, Riley, et al.[22] interpret the photoemission results on amorphous $Pd_{0.81}$ $Si_{0.19}$ in terms of a filling of the Pd 4d shell, and Hines, et. al.[24] have interpreted their NMR data in terms of a filling of the Pt 5d holes in the $(Ni_yPt_{1-y})_{75}P_{25}$ system. Results of saturation magnetic moment measurements are often considered a different form of evidence for d band filling in metallic glasses. Thus, Mizoguchi and Yamauchi[25] interpret the changes in magnetic moment of the 3d transition metal in certain (TM + G) metallic glasses in terms of simple charge transfer from metalloid atoms to the TM 3d holes. Finally, in certain interpretations of the Polk structural model for metallic glasses, the metalloid atoms are thought to transfer charge to the unfilled d band of the transition metal[26,27].

Despite the common assumption of d band filling in TM + G metallic glasses, there is now considerable evidence counter to this view for related crystalline alloys, as well as metallic glasses. Studies of the Ni L_{III} and L_{II} x-ray absorption near edge spectra (XANES) in Ni_yAl_{1-y} and Ni_yCu_{1-y} random solid solutions, as well as in a $Ni_{0.80}P_{0.20}$ metallic glass, show no evidence for filling of Ni 3d holes in the random solid solution studies and little d hole filling in the case of the metallic glass[28,29,30]. In a most striking example of such a study, Rossi, et. al.[31] measured the Pd L_{III} and L_{II} XANES for pure Pd and a number of Pd silicides. They found that in going from Pd to Pd_2Si to PdSi, the number of Pd 4d holes per Pd atom actually increases with silicon concentration. In such investigations, the number of d holes per transition metal site is monitored by measuring the intensity of the sharp absorption peak or "white line" which corresponds to dipole allowed transitions between 2p and unoccupied d states. In the present work, the apparent conflict between the results of XANES and $\rho_d(E_f)$ measurements is shown to be particularly acute for the $(Ni_{0.50}Pt_{0.50})_{75}P_{25}$ system. A model is proposed to resolve the apparent conflict between different types of data.

B. Experimental Apparatus and Procedure

The metallic glass samples were splat quenched foils, manufactured by the piston and anvil technique. The amorphous nature of the samples were confirmed by x-ray diffraction. Data was taken using the C2 beam line of the CHESS synchrotron facility. A channel-cut silicon monochromator crystal with a (220) cut was used. At the Pt edge, the instrumental resolution is estimated to be on the order of 2 eV. In order to test for any influence of the x-ray "thickness effect" on the data, different thicknesses of sample were measured[32,33]. Under the present experimental conditions, it was determined that thickness effects did not significantly influence the spectra.

C. Results and Analysis

Fig. 4 compares the Pt XANES of pure Pt and $(Ni_{0.50}Pt_{0.50})_{75}P_{25}$ for the L_{III} edge. A similar comparison is illustrated in Fig. 5 for the L_{II} edge. Both sets of data are treated by first subtracting the pre-edge background and then normalizing to a node in the extended structure approximately 50 eV above threshold. The pre-edge region of the metallic glass L_{II} edge shows an unexplained spectral feature which consists of an initial rise followed by a dip. Experiments carried out on more Pt rich compositions of the $(Ni_yPt_{1-y})_{75}P_{25}$ system show the amplitude of this feature increasing systematically with Pt concentration, and the dip goes negative in a manner suggestive of the Fano effect[34]. However, until more synchrotron time becomes available so that it is possible to exhaustively reproduce this feature of the data, our emphasis will be on the d band occupancy of the single $(Ni_{0.50}Pt_{0.50})_{75}P_{25}$ composition.

Several methods have been proposed for quantifying XANES spectra in terms of d hole count[35,36,37]. Lytle suggests that an arctangent-like approximation to the continuum be removed in order to isolate the d hole contribution[35]. In Lytle's method, the inflection points of the absorption edge and arctangent are aligned. Brown, et. al.[36], point out that both L_{II} and L_{III} edges must be compared, since these spectra are senstitive to $d_{3/2}$ and $d_{5/2}$ holes, respectively. This consideration is particularly important for Pt XANES because of the relativistic effects in the Pt band structure[38]. One often overlooked point in discussions of how best to subtract the continuum contribution from the XANES is the difficulty of knowing how to align the energy scale of a presumed continuum state arctangent with the observed absorption edge. In Lytle's method, the inflection point of the arctangent is lined up with the inflection point of the experimental spectrum[35]. Traditionally, the inflection point of an absorption edge has been

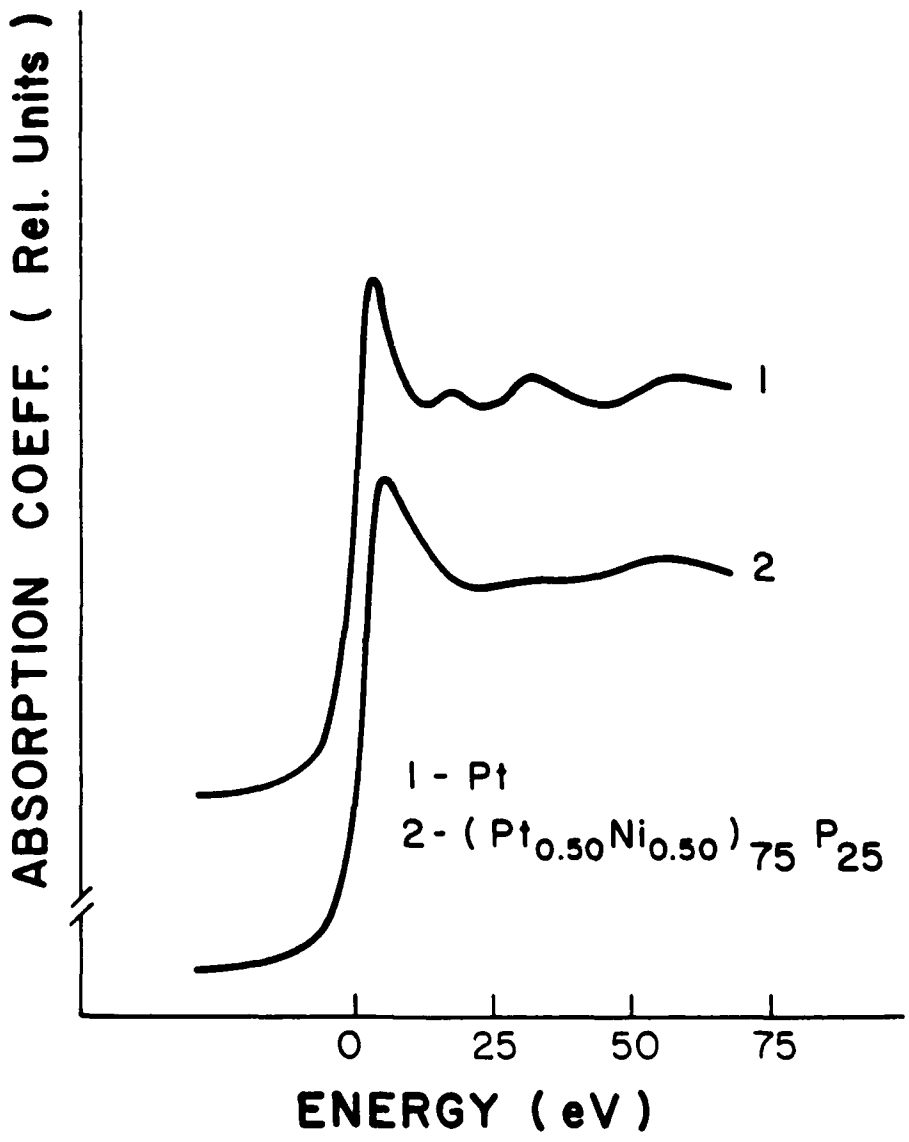

FIGURE 4
Pt L_{III} edges of pure Pt and $(Pt_{0.50}Ni_{0.50})_{75}P_{25}$

taken to be a good measure of the position of the Fermi energy[39]. However, for absorption edges having white lines, the Fermi energy position will not be at the inflection point, but occurs closer to the white line maximum[40]. For the nickel L_{III} edge, the Fermi energy is, in fact, nearly coincident with the peak of the maximum[41]; and in general the position of E_f will not be well known in the absence of a theoretical calculation of the spectrum. Because of the difficulty in knowing just how to align the continuum background on the energy scale, a quantitative measurement of Pt d hole count is not attempted here. However, from inspection, the L_{III} white line of the metallic glass is slightly lowered and broadened relative to that of pure platinum, and the area under this white line is roughly the same in going from Pt to the amorphous alloy. Thus, the number of d holes of 5/2 character per platinum atom does not change significantly in going to the metallic glass. On the other hand, the area under the threshold region of the L_{II} edge is clearly less for pure Pt than for the amorphous material. This difference is sufficiently large, that if one were to use any of the usual schemes in which the d hole count in the L_{II} edge is obtained by subtracting an arctangent-like continuum, the remaining absorption edge area would be greater for the L_{II} edge of the glass than for that of Pt metal. Thus, to the extent that the types of analyses discussed above indeed yield a measure of d hole count, in the present study the number of $d_{5/2}$ holes per Pt site remains about the same and the number of $d_{3/2}$ holes increases in going from Pt to $(Ni_{0.50}Pt_{0.50})_{75}P_{25}$.

D. Discussion and Conclusions

The apparent disagreement between XANES and determinations of $\rho_d(E_f)$ is particularly acute in the case of XANES versus core-polarization Knight shift measurements of $(Ni_{0.50}Pt_{0.50})_{75}P_{25}$, since both experiments sample the electronic structure local to Pt sites. Although it might be tempting

to ascribe this apparent discrepancy to core hole-many body effects in XANES[42], it has by now been demonstrated that band structure calculations of transition metal XANES yield good agreement with experiment, even neglecting core hole-many body effects on the wave functions[41,43]. It is important, however, to take into account lifetime broadening effects in such calculations. For instance, in the L_{III} XANES of nickel, the core hole broadening is so much greater than the actual width of the unoccupied d band that the height of the threshold peak in the XANES is sensitive only to the integrated number of 3d holes and is insensitive to the detailed behavior of the density of states near E_f. This point is of particular importance in the calculation of the Ni_yCu_{1-y} XANES by Munoz, et. al.[44], using the KKR CPA method. Detailed agreement is obtained with the experimental results of Cordts, et. al.[29], even though the calculated $\rho_d(E_f)$ is decreasing rapidly with increasing copper concentration, and the experimental results indicate no corresponding change in the integrated number of 3d holes per nickel site. The calculation shows the high energy tail of the unoccupied d states extending further above the Fermi energy as copper concentration increases. Thus, the calculated area corresponding to the total number of nickel 3d holes per nickel atom does not decrease, though $\rho_d(E_f)$ does decrease as copper concentration becomes larger. In a calculation more germane to the present discussion, Bisi and Calandra[45] have calculated the partial density of Pt d states for crystalline Pt_2Si. The value of $\rho_d(E_f)$ is quite low, though there is a large density of Pt 5d states split off from the main 5d band and peaking about 1 eV above E_f. Since the broadening of the Pt L_{III} core hole is roughly 5 eV[46], XANES of this material would integrate the entire d hole region but be completely insensitive to the low $\rho_d(E_f)$. In conclusion, there is no real discrepancy between XANES and various probes of $\rho_d(E_f)$, for the presently studied system

and others as well. The moral to be drawn is that even if the addition of a metalloid to a TM based glassy alloy results in a lowering of $\rho_d(E_f)$, this observation by no means implies that the d band is being filled in the process.

Finally, it should be mentioned that the present paper has not dealt with yet another potential conflict between XANES and other probes of alloy electronic structure; namely, the extinction of the TM saturation moment in systems for which no d hole filling is detected. There are schematic models of ferromagnetism in these systems which have potential for resolving this difficulty, such as the split band approach of Beeby[47] or the model of Corb, et. al.[48] The nature of the dependence of ferromagnetism on alloying is still a subject requiring considerable experimental and theoretical investigation.

VI. EXAFS STUDY OF METGLAS 2605 CO

A. Introduction

Metglas 2605 CO ($Fe_{67}Co_{18}B_{14}S_1$)[9,49,50] exhibits a high magnetomechanical coupling factor after undergoing specific annealing treatments[9]. In order to investigate the near neighbor atomic environments in this material, and how these environments are affected by the thermal, mechanical, and magnetic history, measurements of both the Fe and Co K-shell extended x-ray absorption fine structure (EXAFS) were carried out in as quenched and magnetically annealed samples. Data were taken at room temperature and liquid nitrogen temperatures, with x-ray polarization directions parallel and perpendicular to the ribbon length. Using the standard techniques of EXAFS data analysis, quantitative information was obtained concerning the first near neighbor (1nn) shell for both Fe and Co atoms. For each of the cases described above (annealing history, temperature and polarization direction), the Fe 1nn distance was larger than that corresponding to Co. Estimates for the fractional disorder parameters were obtained.

B. Experimental Apparatus and Procedure

The x-ray absorption samples were metallographically thinned from both sides to 8-10 μm, such that surface crystallinity[50] was removed. The two types of x-ray absorption samples used in this study were the same as those used in earlier NMR[49] and x-ray diffraction[50] work, and have undergone the following treatments: (i) no annealing treatment after fabrication and thinning and (ii) annealing after thinning for 10 minutes at 369 °C in a magnetic field of 6.1 kOe lying in the plane of the ribbon, transverse to its length. The sample prepared from the original material, (i) above, is designated "as quenched". The sample prepared by process (ii) above is designated "annealed" and yields a value of k_{33} near the maximum obtained for Metglas 2605 CO[9].

The x-ray absorption spectra were measured, with the samples at room temperature, using the EXAFS-I beam line at SSRL and the C2 beam line at CHESS, each equipped with a channel-cut silicon (220) monochromator crystal. Spectra were measured for annealed samples at SSRL, and for both annealed and as quenched samples at CHESS. In addition, spectra were measured with the samples at liquid nitrogen temperature at CHESS.

C. Results and Analysis

All of the spectra were analyzed using the standard procedure which is based on the formalism of Sayers, et al.[51] as modified by Stern and others. EXAFS is defined as the normalized oscillatory part of the absorption coefficient, μ, and is symbolized by $\chi(k)$ where $\chi(k)$ is expressed as

$$\chi(k) = \Sigma_j \frac{(-1)N_j}{kr_j^2} \exp(-2r_j/\lambda)\exp(-2\sigma_j^2k^2)t_j(2k)\sin[2kr_j + \delta_j(k)]. \quad \text{eqn. (1)}$$

In the above expression $k = \sqrt{2m(\varepsilon - \varepsilon_o)/h^2}$ is the wave vector of the photoelectron, the summation is over near neighbor shells, N_j is the number of atoms in the jnn shell, λ is the mean free path of the electron, $t_j(2k)$ is the back scattering amplitude for an atom in the jnn shell, $\delta_j(k)$ is the phase shift function, r_j is the distance to the jnn shell measured from the absorbing atom, and σ_j is a Debye-Waller type factor which gives a measure of the disorder in r_j for the case where deviations from Gaussian disorder have been neglected. $\chi(k)$ is Fourier transformed to yield a radial function, $F(r)$, whose magnitude $|F(r)|$, will peak at $r = R_j$, where R_j is related to the jnn shell distance, r_j, by a shift equal to an average of $d\delta_j(k)/dk$. The amplitude of the peak $|F(R_j)|$, is proportional to $(N_j/\sigma_j r_j^2)$.

Typical transforms of the Fe and Co EXAFS in Metglas 2605 CO are shown in Figs. 6 and 7, respectively. For each transform, the threshold energy, ε_o, has been varied to insure that the maxima in $|F(r)|$ and $Im[F(r)]$ occur

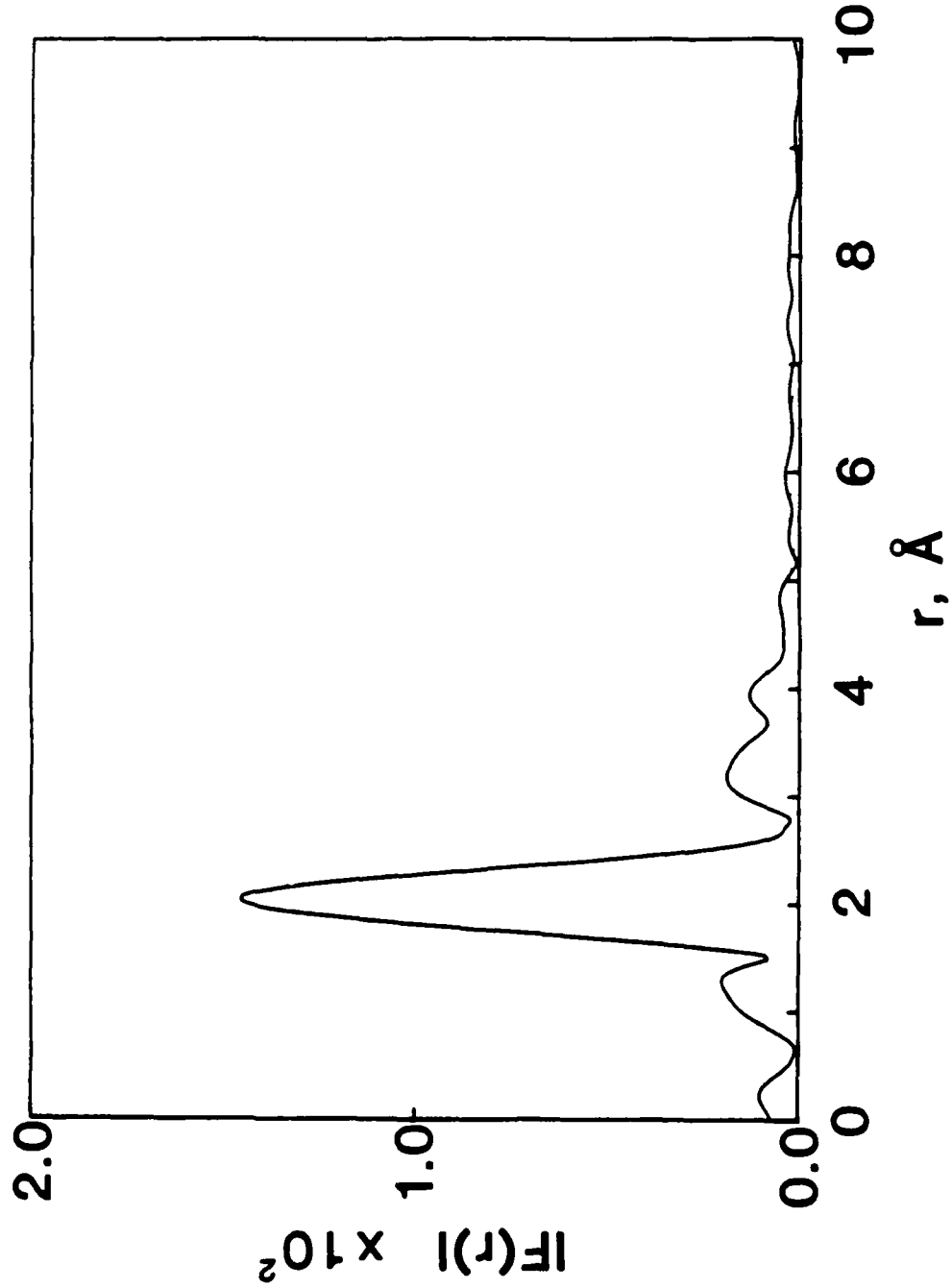

FIGURE 6
Fourier transform of $k^3\chi(k)$ for Fe in as quenched Metglas 2605 CO; room temperature data with x-ray polarization parallel to ribbon length.

FIGURE 7
Fourier transform of $k^3\chi(k)$ for Co in as quenched Metglas 2605 CO; room temperature data with x-ray polarization parallel to ribbon length.

at the same value of r for the 1nn peak. This type of adjustment in ε_o is recommended by Lee and Beni[52] as a means of minimizing errors in R_j caused by uncertainties in the positioning of the threshold energy to a feature of the absorption edge. The positions, R_1, and corresponding amplitudes, $|F(R_1)|$, for the 1nn peak of various Fe and Co transforms, obtained using a k^3-weighting, are summarized in Table II. Two dominant features of the

TABLE II - Position and amplitude of 1nn peak in the magnitude of the k^3 transforms for Metglas 2605 CO.

DATA CASE			Fe Absorber		Co Absorber	
			R_1(Å)	$\|F(R_1)\|$ (Arb. Units)	R_1(Å)	$\|F(R_1)\|$ (Arb. Units)
Room Temperature						
As Quenched:	Parallel	(a)	2.040±0.005	124	2.027±0.005	179
	Parallel	(b)	2.040±0.005	146	2.027±0.005	170
	Perpendicular	(b)	2.040±0.005	130	2.013±0.005	169
Annealed:	Parallel	(a)	2.040±0.005	125	2.027±0.005	182
	Parallel	(b)	2.040±0.005	137	2.027±0.005	184
	Perpendicular	(a)	2.040±0.005	102	2.027±0.005	185
	Perpendicular	(b)	2.040±0.005	138	2.027±0.005	182
Nitrogen Temperature						
As Quenched:	Parallel	(b)	2.040±0.005	166	2.027±0.005	203
	Perpendicular	(b)	2.040±0.005	153	2.027±0.005	212
Annealed:	Parallel	(b)	2.040±0.005	176	2.027±0.005	221
	Perpendicular	(b)	2.040±0.005	162	2.027±0.005	223

(a) data collected at SSRL

(b) data collected at CHESS

data are: (i) R_1 for Fe is consistently larger than R_1 for Co, and (ii) $|F(R_1)|$ for Fe is smaller than $|F(R_1)|$ for Co. Assuming that N_1 and r_1 do not change appreciably with temperature, and using $|F(R_1)| \propto N_1/\sigma_1 r_1^2$, it can be shown that

$$\frac{\Delta\sigma^2}{\sigma_{77K}^2} = \left(\frac{|F(R_1)|_{77K}}{|F(R_1)|_{300K}}\right) - 1, \qquad \text{eqn. (2)}$$

where $\Delta\sigma^2 \equiv \sigma_{300K}^2 - \sigma_{77K}^2$; and σ_{300K} and σ_{77K} are the disorder parameters for the 1nn shell at room temperature and liquid nitrogen temperature, respectively[53]. The values of the fractional change in disorder, $\Delta\sigma^2/\sigma_{77K}^2$, obtained from the corresponding $|F(R_1)|$ values are listed in Table III. The most significant feature of the $\Delta\sigma^2/\sigma_{77K}^2$ values is the anisotropy in the change of local Fe site disorder caused by the magnetic annealing. No qualitative difference occurred in the behavior of $\Delta\sigma^2/\sigma_{77K}^2$ when similar calculations were carried out using k-weighted transforms instead of k^3-weighted transforms.

TABLE III - Fractional change in disorder of Fe and Co sites in Metglas 2605 CO as determined from the k^3 transform data.

DATA CASE		Fe data $\Delta\sigma^2/\sigma^2_{77k}$	Co data $\Delta\sigma^2/\sigma^2_{77k}$
As Quenched:	Parallel	0.293	0.426
	Perpendicular	0.385	0.574
Annealed:	Parallel	0.650	0.443
	Perpendicular	0.378	0.501

D. Discussion and Conclusions

The most notable aspects of the data are that R_1 for Fe is larger than R_1 for Co, and the indication of anisotropy. Several analyses have been carried out to determine if the observed differences in R_1 really indicate

that the average distance of the nearest transition metal shell from an Fe absorber is greater than that from Co. The differences in R_1 between Fe and Co do not seem to be overly sensitive to the choice of ε_0. It has been found that even if the threshold energy is located at the inflection point of the edge, the traditional location of the Fermi energy[39], the Fe transform peaks at a larger r than the Co transform. Values for R_1 were also obtained by plotting the node order of χ as a function of k, in the manner described by Lytle, et al.[51] The plots yield excellent straight line fits, and the R_1 values obtained from the slopes exhibit the same behavior as those listed in Table II. In order to test for the effect of changing the absorbing atom on the EXAFS, model calculations for $\chi(k)$ using eqn. (1) have been carried out with Fe and Co absorbers in identical environments. Theoretical values for the Fe parameters were taken directly from Teo and Lee[54], while interpolated values were used for the Co parameters. These calculations show that the effect of replacing Fe by Co is to shift the peaks in $\chi(k)$ to lower k, which is expected as the Co central atom phase shift is larger than the Fe central atom phase shift. The experimental spectra, however, exhibit the opposite behavior, i.e., the Fe EXAFS peaks are at lower k relative to the corresponding Co EXAFS peaks. In addition, the near edge spectra for Fe and Co in Metglas 2605 CO were compared by aligning the Fermi energies of the respective spectra. It was found that the near edge spectra are quite similar in shape, except that the Fe near edge peaks are shifted to lower k-values relative to the corresponding peaks for Co. This behavior of the near edge spectra is to be expected based upon the differences in R_1 derived from the EXAFS analysis[55].

In order to test for the possible influence of B atoms on the measured differences in R_1, values were obtained using both k- and k^3-weighted transforms. No significant difference was found in the R_1 shifts. Since the B

back scattering amplitude dies out much more rapidly with k than does that of the transition metal, this result is indicative that the shift in R_1 is mainly due to the transition metal environment. Finally, using a model structure based on the Fe_2B and Co_2B crystalline phases, it was found that the R_1 values were dominated by the transition metals. (Since Teo and Lee's work[54] do not include calculations for the B parameters, C parameters were used.)

Perhaps the most difficult aspect of the analysis to deal with is the effect of disorder on the Fe and Co R_1 values. Differences in the R_1 values for Fe and Co could arise from differences in the disorder parameters. Greegor and Lytle[56], in their analysis of fcc Cu, found that an increase in disorder resulted in an apparent decrease in the 1nn distance. A similar result was obtained by Eisenberger and Brown[57] in their study of hcp Zn. In an investigation more germane to the present discussion, De Crescenzi, et al.[58] found that the effect of a large non-Gaussian disorder on the EXAFS of the amorphous $Fe_{80}B_{20}$ system is to produce a shift in the 1nn peak of $|F(r)|$ to lower r with a corresponding decrease in the amplitude. In the present work, if it were to be assumed that the observed difference in R_1 between Fe and Co is a consequence of a larger disorder about the Co sites relative to the Fe sites, the 1nn coordination, N_1, for Co would have to be significantly greater than that for Fe. This conclusion follows from a consideration of the expression for $|F(R_1)|$, i.e., $|F(R_1)| \propto N_1/\sigma r_1^2$, in the light of the values for R_1 (as they related to r_1) as well as the corresponding values for $|F(R_1)|$. Although it is not possible to completely rule out that structural disorder causes the observed differences in the Fe and Co R_1 values, a more likely explanation is based on the known structures of Fe-Co borides. The observed differences in R_1 values for Metglas 2605 CO are in the same direction and of the same

order of magnitude as the change in near neighbor distance for the crystalline $(Fe_{1-x}Co_x)$-borides, in which the lattice parameter decreases with increasing Co concentration, x[59]. On the other hand, the lattice parameter is essentially independent of Co concentration in random solid solutions of $Fe_{1-x}Co_x$ for $0 \leqq x \leqq 0.3$[59]. This indicates that a model based on the dense random packing of Fe and Co spheres would not yield the type of R_1 differences observed in the present experiment.

The largest change in $\Delta\sigma^2/\sigma_{77k}^2$ due to annealing occurs in the direction parallel to the ribbon length for the environment of the Fe sites. One contribution to the observed anisotropy could be stress relief due to annealing[60]. In addition, Egami and others[61] have postulated subtle atomic rearrangements in magnetically annealed metallic glasses originating from the pseudo-dipolar interaction between pairs of Fe atoms. Such effects could contribute to anisotropies in nearest neighbor environments. However, until other studies can be carried out, in which results with and without a magnetic field are compared, the relative importance of the above two mechanisms cannot be ascertained.

VII. OTHER WORK

A. Optical Properties of the Ni-P Metallic Glasses

In order to investigate the electronic structure of the $Ni_{100-x}P_x$ ($15 \leq x \leq 26$) metallic glass system, measurements of the specular reflectivity for near normal incidence have been carried out at room temperature over the energy range 0.52 eV to 6.2 eV on samples prepared by both rapid quenching and electroplating techniques. The measured reflectivity for rapidly quenched $Ni_{81}P_{19}$ decreases from 85% (0.52 eV) to 15% (6.2 eV), with structure occurring at approximately 4.0 eV. The reflectivity behavior is qualitatively similar to that observed for Au-Si metallic glasses, however, a plot of $-\ln_e R$ vs. $E^{1/2}$ for low energies does not follow the (linear) Drude form [62]. Calculations for the real part of the dielectric constant, ε_1, and optical absorption, ε_2/λ, carried out by the standard Kramers-Kronig analysis as well as a "time domain" method were consistent[63]. Similar measurements of the reflectivity have been made on various compositions of electroplated $Ni_{100-x}P_x$ and the results will be discussed in terms of existing models for the electronic structure.

B. Spin-Echo NMR Study of the Atomic Environment in the $Fe_{100-x}B_x$ Metallic Glass System

In order to investigate the near neighbor atomic environments in magnetically ordered transition metal + metalloid metallic glasses, we have utilized spin echo NMR to measure the hyperfine field distribution in the binary $Fe_{100-x}B_x$ system ($14 \leq x \leq 22$). Broad spectra have been obtained at 4.2 °K over the frequency range 26 MHz to 46 MHz. As expected from isotropic abundance and relative NMR sensitivity considerations, and demonstrated by Raj, et al.[64], the principal contribution to the spectra at these frequencies arises from the ^{11}B nuclei and corresponds to a hyperfine field transferred from the near neighbor Fe atoms. The addition of B t

the $Fe_{100-x}B_x$ metallic glass system shifts the peak in the hyperfine field distribution to smaller values. As x increases, intensity is added to the low field portion of the distribution while the high field region remains unchanged. These results, along with ^{57}Fe hyperfine field measurements obtained on this system from Mössbauer experiments[65], will be discussed in the light of existing models for the near neighbor atomic environments.

VIII. PUBLICATIONS ATTRIBUTED TO AFOSR SUPPORT

A. Journal Articles

1. Hines, W. A., K. Glover, W. G. Clark, L. T. Kabacoff, C. U. Modzelewski, R. Hasegawa and P. Duwez. 1980. Electronic structure of the Ni-Pd-P and Ni-Pt-P metallic glasses: A pulsed NMR study. Phys. Rev. B 21:3771.

2. Niculescu, V. A., W. A. Hines, J. I. Budnick, J. Perkins, G. C. Papaefthymiou and T. J. Burch. 1981. A local environment model for the hyperfine interactions in $Fe_{3-x}Ni_xSi$. Phys. Rev. B 23:2388.

3. Hines, W. A., C. U. Modzelewski, R. N. Paolino and R. Hasegawa. 1981. NMR and magnetic susceptibility study of roller quenched $Ni_{100-x}P_x$ metallic glasses. Solid State Commun. 39:699.

4. Hines, W. A., C. U. Modzelewski, R. N. Paolino and H. S. Chen. 1981. NMR and magnetic susceptibility study of melt spun $(Ni_{0.20}Pt_{0.80})_{100-x}P_x$ metallic glasses. J. Appl. Phys. 52:1814.

5. Ford, J. C., W. A. Hines, J. I. Budnick, A. Paoluzi, D. M. Pease, L. T. Kabacoff and C. U. Modzelewski. 1981. Spin-echo NMR study of the atomic site environments in the $Fe_{67}Co_{18}B_{14}Si_1$ metallic glass. J. Appl. Phys. 53:2288.

6. Giessen, B. C., W. A. Hines and L. T. Kabacoff. 1980. Magnetic properties of amorphous $RE_{65}Al_{35}$ alloys. IEEE Trans. on Magnetics, MAG-16:1203.

7. O'Handley, R. C., B. W. Corb, Y. Hara, N. J. Grant and W. Hines. 1982. Magnetic properties of some new Co-Nb-B metallic glasses. J. Appl. Phys. 53:7753.

8. Hines, W. A., P. Miller, A. Paoluzi, C. L. Tsai and B. C. Giessen. 1982. NMR and magnetic susceptibility study of the $Ca_{100-x}Al_x$ metallic glass system. J. Appl. Phys. 53:7789.

9. Choi, M., D. M. Pease, W. A. Hines, J. I. Budnick, G. H. Hayes and L. T. Kabacoff. 1983. A study of the crystalline surface of Metglas 2605 CO. J. Appl. Phys. 54:4193.

10. Hines, W. A., A. Paoluzi, J. I. Budnick, W. G. Clark and C. L. Tsai. 1984. Atomic and electronic structures of the Ca-Al metallic glass system: a pulse NMR study. J. Non-Cryst. Solids.

11. Pease, D. M., G. H. Hayes, M. Choi, J. I. Budnick, W. A. Hines, R. Hasegawa and S. M. Heald. 1984. On the density of unoccupied d states in transition metal - metalloid metallic glasses. J. Non-Cryst. Solids.

B. Abstracts

1. Hines, W. A., R. N. Paolino, W. G. Clark, K. Glover and R. Hasegawa. 1980. NMR and magnetic susceptibility study of roller quenched $Ni_{100-x}P_x$ metallic glasses. Bull. Am. Phys. Soc. 25:273.

2. O'Handley, R. C., B. Corb, N. J. Grant, W. Hines and S. Foner. 1982. Magnetic properties of some new Co-Nb-B metallic glasses. Bull. Am. Phys. Soc. 27:411.

3. O'Handley, R. C., B. Corb, N. J. Grant and W. Hines. 1982. Magnetic properties of some new Co-Nb-B metallic glasses. Rapid Solidification Processing Workshop, M.I.T., April 22-23, 1982, p. 24.

4. Yang, D., W. A. Hines, C. W. Peterson, G. Coutu and H. E. Schone. 1983. Optical properties of the Ni-P metallic glasses. Bull. Am. Phys. Soc. 28:484.

5. Hines, W. A., W. G. Clark and C. L. Tsai. 1983. Pulsed NMR study of the Ca-Al metallic glass system. Bull. Am. Phys. Soc. 28:485.

6. Choi, M., D. M. Pease, W. A. Hines, J. I. Budnick and G. H. Hayes. A study of the crystalline surface of Metglas 2605 CO. Bull. Am. Phys. Soc. 28:529.

7. Hayes, G. H., J. I. Budnick, M. Choi, W. A. Hines, D. M. Pease, D. E. Sayers and S. M. Heald. 1983. X-ray absorption study of Metglas 2605 CO. Bull. Am. Phys. Soc. 28:862.

C. Oral Presentations

1. Institute of Chemical Analysis, Northeastern University
Materials Science Seminar
November 7, 1979

2. Materials Research Society
1979 Annual Meeting, Cambridge, Massachusetts
November 28, 1979

3. Department of Physics, University of Connecticut
Physics Colloquium
February 1, 1980

4. American Physical Society
New York Meeting
March 25, 1980

5. Department of Physics, College of William and Mary
Physics Colloquium
April 16, 1980

6. Department of Physics and Physical Sciences, Virginia Commonwealth University
Seminar and Colloquium Series
April 17, 1980

7. 25th Annual International Magnetics Conference
Boston, Massachusetts
April 24, 1980

8. 26th Annual Conference on Magnetism and Magnetic Materials
   Dallas, Texas
   November 13, 1980

9. Naval Surface Weapons Center
   Solid State Seminar
   May 13, 1981

10. Department of Physics, University of Delaware
    Solid State Seminar
    May 14, 1981

11. 27th Annual Conference on Magnetism and Magnetic Materials
    Atlanta, Georgia
    November 10, 1981

12. 3rd Joint Intermag. - Magnetism and Magnetic Materials Conference
    Montreal, Quebec, Canada
    July 22, 1982

13. Institute of Chemical Analysis, Northeastern University
    Materials Science Seminar
    February 23, 1983

14. Department of Physics, Northeastern University
    Physics Colloquium
    February 23, 1983

15. American Physical Society
    Los Angeles Meeting
    March 24, 1983

16. 5th International Conference on Liquid and Amorphous Metals
    Los Angeles, California
    August 15, 1983

17. Institute of Materials Science, University of Connecticut
    Advisory Board Meeting
    October 31, 1983

18. Department of Physics, University of Rhode Island
    Physics Colloquium
    November 11, 1983

IX. COURSE OF FUTURE WORK

A. This Coming Year (October 1, 1983 to September 30, 1984)

During the coming year, which is the fifth and final year of the supported research program, the preliminary work described in Section VIIA ("Optical Properties of the Ni-P Metallic Glasses") and Section VIIB ("Spin-Echo NMR Study of the Atomic Environment in the $Fe_{100-x}B_x$ Metallic Glass System") will be extended to completion. Finally, low temperature specific heat capacity measurements will be performed on the $Ni_{100-x}P_x$ and $Ca_{100-x}Al_x$ metallic glass systems. From the electronic term, which is linear with temperature, direct calculations for the density of states will be carried out.

B. Long Range Goals

The long range objectives beyond the supported research program include an extension of the experimental techniques mentioned above to other amorphous metallic systems. Such systems will be selected from the already explored transition metal + metalloid and metal + metal families as well as the unexplored noble metal + metalloid, transition metal + transition metal and transition metal + rare earth families. As indicated earlier, we feel that the recently available systems consisting of "simple" metals only are a particularly fruitful area for research. The most recent summary of known amorphous metallic systems is provided by Chen[66]. Although some of the systems have nuclear species which are not as favorable for NMR as the ^{31}P, ^{195}Pt, ^{27}Al, ^{11}B and ^{59}Co nuclei in the systems being studied initially, adequate resonance spectra can be obtained by: (1) using a time average computing technique, (2) operating at liquid helium temperatures, (3) using enriched isotopes and (4) dissolving a small amount of favorable nuclear species ($\sim$ 0.1 to 1.0 at. %) into the system which does not alter the basic properties. All of the procedures described above have been employed in

the past with reasonable success. In addition, experiments related to the transport properties (i.e., thermal conductivity and Hall effect) would be utilized in the investigation of the electronic structure and its relationship to physical properties.

REFERENCES

1. Glassy Metals I, edited by H. -J. Guntheradt and H. Beck (Springer-Verlag, New York, 1981).

2. Amorphous Magnetism, edited by F. E. Luborsky (Butterworths, London, 1983).

3. Glassy Metals: Magnetic, Chemical and Structural Properties, edited by R. Hasegawa (CRC Press, Boca Raton, 1983).

4. Proceedings of the Fourth International Conference on Rapidly Quenched Metals, Vols. I and II, edited by T. Masumoto and K. Suzuki (Japan Institute of Metals, Sendai, 1982).

5. S. R. Nagel and J. Tauc, Phys. Rev. Lett. 35, 380 (1975).

6. R. Ferrer and M. J. Zuckermann, Can. J. Phys. 56, 1098 (1978).

7. K. H. J. Buschow, Solid State Commun. 27, 275 (1978).

8. W. A. Hines, A. H. Menotti, J. I. Budnick, T. J. Burch, T. Litrenta, V. Niculescu and K. Raj, Phys. Rev. B. 13, 4060 (1976).

9. C. U. Modzelewski, H. T. Savage, L. T. Kabacoff and A. E. Clark, IEEE Trans on Magnetics, MAG-17, 2837 (1981).

10. C. D. Graham and T. Egami, Ann. Rev. Mater. Sci. 8, 423 (1978).

11. W. A. Hines, P. Miller, A. Paoluzi, C. L. Tsai and B. C. Giessen, J. Appl. Phys. 53, 7789 (1982).

12. R. Pond and R. Maddin, Trans. Met. Soc. AIME 245, 2475 (1969).

13. J. A. McNeil and W. G. Clark, Rev. Sci. Instrum. 44, 844 (1973).

14. Y. H. Yun and J. P. Bray, J. Non-Cryst Solids 30, 45 (1978) and references therein.

15. R. G. Barnes, W. H. Jones and T. P. Graham, Phys. Rev. Letters 6, 221 (1961).

16. P. Panissod, D. Aliaga Guerra, A. Amamou, J. Durand, W. L. Johnson, W. L. Carter and S. J. Poon, Phys. Rev. Letters 44, 1465 (1980).

17. P. Panissod, I. Bakonyi and R. Hasegawa, Phys. Rev. B, to be published.

18. S. R. Nagel, U. M. Gubler, C. F. Hague, J. Krieg, R. Lapka, P. Oelkafen, H. -J. Güntherodt, J. Evers, A. Weiss, V. L. Moruzzi and A. R. Williams, Phys. Rev. Letters 49, 575 (1982).

19. S. R. Nagel, G. B. Fisher, J. Tauc and B. G. Bagley, Phys. Rev. B 13, 3284 (1976).

20. B. G. Bagley and F. J. DiSalvo, in Amorphous Magnetism, edited by H. O. Hooper and A. M. de Graaf (Plenum, New York, 1973), p. 143.

21. B. Golding, B. G. Bagley, and F. S. L. Hsu, Phys. Rev. Lett. 29, 68 (1972).

22. J. D. Riley, L. Ley, J. Azoulay and K. Terakura, Phys. Rev. B 20, 776 (1979).

23. W. A. Hines, C. U. Modzelewski, R. N. Paolino and R. Hasagawa, Solid State Commun. 39, 699 (1981).

24. W. A. Hines, L. T. Kabacoff, R. Hasegawa and P. Duwez, in Amorphous Magnetism, edited by R. A. Levy and R. Hasegawa (Plenum, New York, 1977), p. 207.

25. T. Mizoguchi, K. Yamuchi and H. Miyajima, in Amorphous Magnetism, edited by H. O. Hooper and A. M. de Graaf (Plenum, New York, 1973), p. 325.

26. D. E. Polk, Acta Metallurgical 20, 485 (1972).

27. C. C. Tsuei, in Amorphous Magnetism, edited by H. O. Hooper and A. M. de Graaf (Plenum, New York, 1973), p. 299.

28. D. M. Pease, L. V. Azaroff, C. K. Vaccaro and W. A. Hines, Phys. Rev B 19, 1576 (1979).

29. B. Cordts, D. M. Pease and L. V. Azaroff, Phys. Rev. B 22, 4692 (1980).

30. E. Belin, C. Bonnelle, J. Flechon, and F. Machizaud, J. Non Cryst. Solids 41, 219 (1980).

31. G. Rossi, R. Jaeger, J. Stöhr, T. Kendelewicz and I. Lindau, Phys. Rev. B 27, 5154 (1983).

32. L. G. Parratt, C. F. Hampstead and E. L. Jossen, Phys. Rev. 105, 1228 (1957).

33. D. M. Pease, Appl. Spectrosc. 30, 405 (1976).

34. U. Fano, Phys. Rev. 124, 1866 (1961).

35. F. W. Lytle, J. Catal. 43, 376 (1976).

36. M. Brown, R. E. Peierls and E. A. Stern, Phys. Rev. B 15, 738 (1977).

37. J. A. Horsley, J. Chem. Phys. 76, 1451 (1982).

38. L. F. Mattheiss and R. E. Dietz, Phys. Rev. B 22, 1663 (1980).

39. F. K. Richtmyer, S. W. Barnes and E. Ramberg, Phys. Rev. 46, 843 (1934).

40. D. M. Pease and L. V. Azaroff, J. Appl. Phys. 50, 6605 (1979).

41. F. Szmulowicz and D. M. Pease, Phys. Rev. B 17, 3341 (1978).

42. G. D. Mahan, in Solid State Physics, Vol. 29, edited by H. Ehrenreich, F. Seitz and D. Turnbull (Academic, New York, 1974), p. 75.

43. J. E. Müller, O. Jepsen and J. W. Wilkens, Solid State Commun 42, 365 (1982).

44. M. C. Munoz, P. J. Durham and B. L. Gyorffy, J. Phys. F: Met. Phys. 12, 497 (1982).

45. O. Bisi and C. Calandra, J. Phys. C. Solid State Phys. 14, 5479 (1981).

46. M. H. Chen, B. Crasemann and H. Mark, Phys. Rev. A 24, 177 (1981).

47. J. L. Beeby, Phys. Rev. 141, 781 (1966).

48. B. W. Corb, R. C. O'Handley and N. J. Grant, Phys. Rev. B 27, 636 (1983).

49. J. C. Ford, W. A. Hines, J. I. Budnick, A. Paoluzi, D. M. Pease, L. T. Kabacoff and C. U. Modzelewski, J. Appl. Phys. 53, 2288 (1982).

50. M. Choi, D. M. Pease, W. A. Hines, J. I. Budnick and G. H. Hayes, J. Appl. Phys. 54, 4193 (1983).

51. F. W. Lytle, D. E. Sayers and E. A. Stern, in Advances in X-Ray Spectroscopy, edited by C. Bonnelle and C. Mandé (Pergamon, Oxford, 1982), p. 267.

52. P. A. Lee and G. Beni, Phys. Rev. B 15, 2862 (1977).

53. J. Wong, F. W. Lytle, R. B. Greegor, H. H. Liebermann, J. L. Walter and F. E. Luborsky, in Rapidly Quenched Metals III, Vol. 2, edited by B. Cantor (Cameleon Press, London, 1978), p. 345.

54. B. K. Teo and P. A. Lee, J. Am. Chem. Soc. 101, 2815 (1979).

55. B. Cordts, D. Pease and L. V. Azaroff, Phys. Rev. B 24, 538 (1981).

56. R. B. Greegor and F. W. Lytle, Phys. Rev. B 20, 4902 (1979).

57. P. Eisenberger and G. Brown, Solid State Commun. 29, 481 (1979).

58. M. De Crescenzi, A. Balzarotti, F. Comin, L. Incoccia, S. Mobilio and N. Motta, Solid State Commun. 37, 921 (1981).

59. W. B. Pearson, Handbook of Lattice Spacings and Structures of Metal (Pergamon Press, New York, 1958).

60. J. Egami and P. J. Flanders, A.I.P. Conf. Proc. 29, edited by J. J. Becker, G. H. Lander and J. J. Phyne (Am. Inst. Physics, New York, 1976), p. 121; I. C. Baianu, J. Patterson and K. A. Rubinson, Mat. Sci. Eng. 40, 273 (1979).